Highlights

- The escape ratio of near-infrared SIF can be estimated using NIR_V and fPAR.
- The approach applies broadly, including sparse canopies with bright soil backgrounds.
- The approach allows estimation of total emitted SIF from directional SIF data.

A practical approach for estimating the escape ratio of near-infrared solar-induced chlorophyll fluorescence

Yelu Zeng[a,b,*,+], Grayson Badgley[a,c,+], Benjamin Dechant[d], Youngryel Ryu[d,e], Min Chen[f], and Joseph A. Berry[a]

[a]Department of Global Ecology, Carnegie Institution for Science, Stanford, CA 94305, USA

[b]State Key Laboratory of Remote Sensing Science, Institute of Remote Sensing and Digital Earth, Chinese Academy of Sciences, Beijing 100101, China

[c]Department of Earth System Science, Stanford University, Stanford, CA 93405, USA

[d]Research Institute of Agriculture and Life Sciences, Seoul National University, Seoul, Republic of Korea

[e]Department of Landscape Architecture and Rural Systems Engineering, Seoul National University, Seoul, Republic of Korea

[f]Joint Global Change Research Institute, Pacific Northwest National Laboratory, College Park, MD, USA

[*]zengyelu@163.com

[+]These authors contributed equally

July 23, 2019

Abstract

Solar-induced chlorophyll fluorescence (SIF) has emerged as a leading approach for remote sensing of gross primary productivity (GPP). While SIF has an intrinsic, underlying relationship with canopy light capture and light use efficiency, these physiological relationships are obscured by the fact that satellites observe a small and variable fraction of total emitted canopy SIF. Upon

emission, most SIF photons are reabsorbed or scattered within the canopy, preventing their observation remotely. The complexities of the radiative transfer process, which vary across time and space, limit our ability to reliably infer physiological processes from SIF observations. Here, we propose an approach for estimating the the fraction of total emitted near-infrared SIF (760 nm) photons that escape the canopy by combining the near-infrared reflectance of vegetation (NIR_V) and the fraction of absorbed photosynthetically active radiation (fPAR), two widely available remote sensing products. Our approach relies on the fact that NIR_V is resilient against soil background contamination, allowing us to reliably calculate the bidirectional reflectance factor of vegetation, which in turn conveys information about the escape ratio of SIF photons. Our NIR_V-based approach explains variations in the escape ratio with an R^2 of 0.91 and an RMSE of 1.48% across a series of simulations where canopy structure, soil brightness, and sun-sensor-canopy geometry are varied. The approach is applicable to conditions of low leaf area index and fractional vegetation cover. We show that correcting for the escape ratio of SIF using NIR_V provides robust estimates of total emitted SIF, providing for the possibility of studying physiological variations of fluorescence yield at the global scale.
Keywords: solar-induced chlorophyll fluorescence, near-infrared reflectance, canopy structure, escape ratio, spectral invariant properties

1 Introduction

The empirical relationship between solar-induced chlorophyll fluorescence (SIF) and gross primary productivity (GPP) is complicated by the fact that we only observe a fraction of emitted SIF photons and that this fraction depends on the direction of observation (Porcar-Castell et al., 2014). It is difficult, therefore, to distinguish physiological variations in the raw SIF signal from variations in SIF caused by radiative transfer processes. Our goal here is to use multispectral remote sensing observations to estimate the total amount of SIF emitted by the chlorophyll of a canopy and to explore the use of this measurement for interpreting canopy scale photosynthesis and light capture.

Many of the challenges of SIF radiative transfer have already been addressed in models (e.g., van der Tol et al. 2009). Such models provide a platform for simulation of chlorophyll to leaf scaling of SIF (Ramos and Lagorio, 2006; Vilfan et al., 2016), the reabsorption of SIF within the leaf

and canopy (Gitelson et al., 1998; Romero et al., 2018), the directionality of SIF emissions from the canopy (Hernández-Clemente et al., 2017; Zhao et al., 2016), and the atmospheric scattering of SIF (Frankenberg et al., 2011a). Yet there does not exist an accepted, broadly applicable way to measure the fraction of the total leaf-level SIF emission that makes its way to the top of the canopy and, ultimately, to the SIF sensor.

The challenge posed by these leaf-to-canopy scale radiative processes is best thought of from a physical standpoint, where SIF, as observed at the top of canopy ($\mathrm{SIF_{Obs}}$), is defined in terms of total emitted SIF ($\mathrm{SIF_{Total}}$):

$$SIF_{Total}(\lambda_f) = PAR \cdot fPAR_{chl} \cdot \Phi_F(\lambda_f), \tag{1a}$$

$$SIF_{Obs}(\lambda_f, \Omega) = SIF_{Total} \cdot f^{esc}(\lambda_f, \Omega). \tag{1b}$$

This formulation explicitly decouples the leaf-level input variables that generate SIF (Eq. 1a) from the canopy radiative transfer processes that govern the fraction of $\mathrm{SIF_{Total}}$ that ultimately escapes the canopy for detection (Eq. 1b). More specifically, $\mathrm{SIF_{Total}}$, defined as the sum of all SIF photons at a given wavelength (λ_f) emitted by all leaves within the canopy in all directions, depends on: i) PAR, photosynthetically active radiation, ii) $fPAR_{chl}$, the fraction of PAR absorbed by chlorophyll, and iii) Φ_F, the quantum yield of fluorescence. Upon emission from the leaf, the photons which comprise $\mathrm{SIF_{Total}}$ are scattered through the canopy and only a fraction, $f^{esc}(\Omega)$, ultimately escape the canopy and are observed at the view angle Ω. Eq. 1 makes clear that detecting meaningful variations in physiology (e.g., changes in Φ_F) from measurements of $\mathrm{SIF_{Obs}}$ requires first accounting for changes in $f^{esc}(\Omega)$.

Quantifying f^{esc} is a complicated task that requires three types of information: i) sun-sensor geometry, ii) canopy structural parameters (e.g., leaf area index, clumping index, and leaf angle distribution), and iii) leaf optical properties (e.g., leaf reflectance/transmittance). Each of these parameters must be known to accurately describe the radiative transfer of SIF. If these data are available, there are numerous physically based forward modeling techniques capable of precisely calculating f^{esc} and thereby quantifying both $\mathrm{SIF_{Obs}}$ and $\mathrm{SIF_{Total}}$ (He et al., 2017; Hernández-Clemente et al., 2017; van der Tol et al., 2009; Zhao et al., 2016). Despite the success of these efforts, the critical parameters for directly calculating f^{esc} are rarely well-characterized at the

site level, let alone at scales relevant to remote sensing. As a result, f^{esc} is treated as constant (e.g., Guanter et al. 2014) or calculated by making *a priori* assumptions that in turn introduce errors into the calculation of f^{esc}. In fact, only a handful of studies have seriously considered the effects of f^{esc} on SIF (e.g., Fournier et al., 2012; Migliavacca et al., 2017; van der Tol et al., 2016), though the subject has recently gained more attention (Liu et al., 2018; Yang and van der Tol, 2018).

Alternatively, it is possible to use the shape of the bidirectional reflectance factor (BRF) derived from reflectance-based measurements to calculate the angular distribution of SIF radiance and thereby calculate $\mathrm{SIF_{Total}}$. BRF-based approaches rely on the fact that solar and SIF photons of the same wavelength are confronted by roughly the same canopy radiative environment, despite originating from distinct physical processes. As a result, it should be possible to use directional information from optical measurements to correct the directional dependencies of SIF. Liu et al. (2016) used this approach and found a strong linearity between bidirectional SIF radiance and the total scene near-infrared bidirectional reflectance factor ($\mathrm{BRF_T}$). Similarly, Yang and van der Tol (2018) showed that for near-infrared SIF, f^{esc} can be described as a function of NIR reflectance, canopy directional interceptance (i_0), and leaf albedo (ω).

The $\mathrm{BRF_T}$ approach for estimating f^{esc} is both computationally and theoretically simple, requiring few inputs outside of multi-spectral $\mathrm{BRF_T}$ measurements (Yang and van der Tol, 2018). Despite these advantages, the $\mathrm{BRF_T}$ approaches, like those developed by Liu et al. (2018) and Yang and van der Tol (2018), implicitly assume that the contribution of photons scattered by the soil is negligible. This assumption holds for SIF, as the SIF signal is specific to vegetation; soil simply cannot emit SIF photons. However, the assumption of minimal soil influence does not hold for reflected sunlight, as solar photons are strongly scattered by the soil. As a result, the $\mathrm{BRF_T}$ approach for estimating f^{esc} can only be used i) over dense canopies, where both the leaf area index (LAI) and fractional vegetation cover (FVC) are high or ii) where soil reflectance is low.

Here, we propose a new BRF-based approach for calculating f^{esc} using the NIR reflectance of vegetation ($\mathrm{NIR_V}$). From a theoretical standpoint, $\mathrm{NIR_V}$ represents the fraction of reflected NIR light that originates from vegetation. In this sense, it attempts to replicate the specificity SIF has to vegetation. In practice, $\mathrm{NIR_V}$ minimizes the influence of soil reflectance on the retrieved reflectance value (Badgley et al., 2017). This enables accurate retrievals of the contribution of vegetation to observed NIR reflectance under a wide array of field conditions, including over sparse

canopies and regardless of soil brightness. As a result, $\mathrm{NIR_V}$ better satisfies the assumption that soil only negligibly contributes to total scene reflectance and thereby provides the basis for a computationally simple and physically-grounded approach for determining the f^{esc} of near-infrared SIF and, as a result, total emitted SIF.

We introduce the approach in four parts, beginning first with an explicit theoretical derivation relating $\mathrm{NIR_V}$ and fPAR to f^{esc}. Second, we use both a one-dimensional and a three-dimensional radiative transfer model to demonstrate the robustness of our proposed model of f^{esc} regardless of solar angle, view angle, soil brightness, and canopy structure. Third, using satellite observations of SIF and NIR reflectance, we directly compare the relationship between SIF-$\mathrm{NIR_V}$ and SIF-$\mathrm{NIR_T}$ across a wide range of ecosystem types to test the empirical usefulness of both measurements as the basis for estimating f^{esc}. Finally, we demonstrate how $\mathrm{NIR_V}$ and fPAR can be used to translate virtual satellite observations of SIF ($\mathrm{SIF_{Obs}}$) into robust measurements of total emitted SIF ($\mathrm{SIF_{Total}}$).

2 Motivation & Theoretical Derivation

Our approach for estimating $\mathrm{SIF_{Total}}$ from measurements of $\mathrm{SIF_{Obs}}$ (Eq. 1) takes its motivation from the recent empirical result by Badgley et al. (2017), which showed that the near-infrared reflectance of vegetation ($\mathrm{NIR_V}$) is strongly correlated with satellite-measurements of $\mathrm{SIF_{Obs}}$ in the near-infrared (740–760 nm) range, which we denote here as $\mathrm{SIF_N}$. Such a strong empirical correspondence between reflected light and SIF indicates that the scattering of reflected near-infrared solar photons and emitted near-infrared $\mathrm{SIF_N}$ are strongly related, a result that has been separately demonstrated from radiative transfer modeling (van der Tol et al., 2016; Yang and van der Tol, 2018). In terms of the task at hand, the correlation between $\mathrm{SIF_N}$ and $\mathrm{NIR_V}$ presents the possibility of using $\mathrm{NIR_V}$ as an independent basis for estimating f^{esc} of $\mathrm{SIF_N}$. Note, the approach discussed for the remainder of the manuscript only pertains to near-infrared measurements of SIF.

The intuition underlying the link between $\mathrm{NIR_V}$ and $\mathrm{SIF_N}$ is best illustrated by considering $\mathrm{NIR_V}$ as a corresponding radiance, $\mathrm{NIR}_V^{'}$:

$$SIF_N = S_{400\text{-}700} \cdot i_0 \cdot \Phi_F \cdot f_N^{esc}, \tag{2a}$$

$$NIR_V^{'} = S_{760} \cdot i_0 \cdot \omega_N \cdot f_N^{esc}. \tag{2b}$$

Eq. 2b represents the total NIR *radiance* reflected by the vegetated component of the land surface, which is a real, measurable flux. Expressing $\mathrm{NIR_V}$ in this way emphasizes that $\mathrm{SIF_N}$ and NIR radiance are strongly related to each other, as both are jointly dependent on the flux of incoming solar radiation, denoted S_{λ_f} ($S_{400\text{-}700}$, or PAR, in the case of SIF; S_{760} for $\mathrm{NIR}_V^{'}$), the fractional interceptance of vegetation (i_0, dependent on canopy gap fraction), and the fraction of photons that escape from the canopy (f_N^{esc}). Eq. 2a differs slightly from the definition of SIF presented in Eq. 1a, as $\mathrm{i_0}$ is not strictly equal to $\mathrm{fPAR_{chl}}$. However, as discussed below, the two are strongly related and writing Eq. 2a in terms of $\mathrm{i_0}$ emphasizes the similarity of SIF to $\mathrm{NIR}_V^{'}$.

While similar, Eq. 2 makes it clear that $\mathrm{SIF_N}$ and $\mathrm{NIR_V}$ are not identical. In particular, SIF and $\mathrm{NIR_V}$ originate from different physical processes within the canopy. SIF photons, on the one hand, are controlled by a biochemically mediated conversion of absorbed light to fluorescence, termed fluorescence yield and denoted as Φ_F. $\mathrm{NIR_V}$, on the other hand, results from the scattering of solar photons by interaction with leaves, making $\mathrm{NIR_V}$ dependent on the leaf single scattering albedo in the NIR band (ω_N). The difference in the origin of the SIF and $\mathrm{NIR_V}$ signals means that the f^{esc} of SIF does not strictly equal the f^{esc} of $\mathrm{NIR_V}$. This is because the contribution of any one leaf to the top of canopy SIF or $\mathrm{NIR_V}$ signal depends on the value of Φ_F or ω_N of that leaf. More specifically, at a given location in the canopy, f^{esc} of SIF and $\mathrm{NIR_V}$ are indeed the same (when neglecting higher order terms for SIF excitation). However, when averaging over the whole canopy, each leaf is weighted by its respective value of either Φ_F or ω_N, causing slight differences in the two canopy-level f^{esc} terms. There are similar, small differences in the penetration of solar PAR and NIR photons within the canopy that drive both SIF and $\mathrm{NIR_V}$. Yet given the strong empirical relationship between $\mathrm{SIF_N}$ and $\mathrm{NIR_V}$, as well as the small relative variability of Φ_F at the leaf-level (van der Tol et al., 2014), it stands to reason that such differences are negligible (though not ignorable). Thus, it should be possible to use $\mathrm{NIR_V}$ to independently estimate f^{esc} and thereby correct for view-angle and within-canopy radiative transfer processes that mediate the relationship between $\mathrm{SIF_{Obs}}$ and $\mathrm{SIF_{Total}}$. The remainder of this manuscript explores that possibility.

2.1 Calculating $\mathrm{BRF_T}$ in the NIR Band

We begin our derivation with the definition of the total scene bidirectional reflectance factor at wavelength λ_f ($\mathrm{BRF_T}(\lambda_f)$), which can be broken down as a linear combination of three parts:

$$BRF_T(\lambda_f) = BRF_V(\lambda_f) + BRF_S(\lambda_f) + BRF_M(\lambda_f). \tag{3}$$

The three components of $\mathrm{BRF_T}$ are: i) $\mathrm{BRF_V}$, the contribution of photons at wavelength λ_f reflected off only the scene's vegetative component, ii) $\mathrm{BRF_S}$, the contribution of photons at wavelength λ_f reflected off soil alone, and iii) $\mathrm{BRF_M}$ which represents the contribution to $\mathrm{BRF_T}$ from multiple scattering between the vegetation and soil.[1] In practice, however, satellites are only capable of measuring $\mathrm{BRF_T}$, as satellites capture light reflected by vegetative and non-vegetative elements alike. For studying vegetation, we are primarily interested in $\mathrm{BRF_V}$, which describes how viewing geometry, canopy structure, and leaf spectral properties influence the scattering of both solar (reflected) and SIF (emitted) photons within the canopy.

More formally, $\mathrm{BRF_V}$ can be described as:

$$BRF_V(\lambda_f) = i_0 \cdot \omega_{\lambda_f} \cdot f^{esc}_{\lambda_f}, \tag{4}$$

where i_0 is canopy interceptance, which represents the probability of a solar photon (of any wavelength) interacting with the canopy and is defined as one minus the directional gap fraction (Smolander and Stenberg, 2005), ω_{λ_f} is the leaf single scattering albedo at wavelength λ_f, and $f^{esc}_{\lambda_f}$ is the fraction of photons at wavelength λ_f that escape the canopy and are detected remotely (Knyazikhin et al., 2013). Yet without prior information on $\mathrm{BRF_S}$ and $\mathrm{BRF_M}$, the task of disentangling $\mathrm{BRF_V}$ from $\mathrm{BRF_T}$ becomes challenging (Eq. 3).

For the problem at hand, we are interested in isolating the $\mathrm{BRF_V}$ in the NIR region, as this is the portion of $\mathrm{BRF_T}$ that contains relevant information about f^{esc}. For convenience, we rewrite Eq. 3 to explicitly consider the NIR case as:

$$NIR_T = NIR_V + NIR_S + NIR_M. \tag{5}$$

In the most straightforward terms, we are interested in calculating the fraction of $\mathrm{NIR_T}$ that originates from interactions with vegetation alone. We can call this fraction F_V. By extension, it is possible to write:

[1] Please see the Glossary for a full listing of terms and abbreviations.

$$F_V + F_S + F_M = 1, \tag{6}$$

meaning that reflectance from vegetation, soil, and the multiple scattering between the two constitute the full NIR_T signal. For the purpose of simplifying the remainder of the derivation, we treat F_M as 0, though subsequent radiative transfer experiments contained within this manuscript make no such assumption.

With Eqs. 5 and 6 in hand, we can write:

$$\begin{aligned} NIR_V &= F_V \cdot NIR_T \\ NIR_S &= F_S \cdot NIR_T \end{aligned} \tag{7}$$

The challenge now becomes finding an appropriate means of estimating NIR_V from measurements of NIR_T. When framed in this way, the challenge posed by Eq. 7 closely parallels the approach used to estimate SIF from remote sensing, which ultimately hinges on determining the fraction of SIF contained within measurements of NIR_T.

One theoretical solution to isolating NIR_V from NIR_T was formulated by Knyazikhin et al. (1998) in what they termed the "black soil problem." The black soil problem states that calculating NIR_V (or BRF_V at any wavelength, for that matter) would be trivial if the canopy was illuminated from above and, instead of being backed by a soil with its own reflectance properties, the soil was replaced by a perfectly absorbent (black) background. In this scenario, both NIR_S and NIR_M become zero and the retrieved NIR_T signal can be safely attributed to vegetation. While such a substitution is impossible in practice, it may be possible to use radiative transfer simulations to identify optical-based vegetation indices that behave similar to NIR_T under black soil conditions.

2.2 An approximation of NIR_V

Here, we explore an approach for approximating NIR_V first described by Badgley et al. (2017):

$$NIR_V \approx NDVI \cdot NIR_T, \tag{8}$$

where NDVI is the normalized difference vegetation index, which depends on red (630–690 nm) and NIR reflectance (750–900 nm) (Tucker, 1979). Eq. 8 makes it clear that the product of NDVI and $\mathrm{NIR_T}$ is an approximation of the proportion of reflected photons that directly interact with vegetation, which is a real, physical property of the scene. It is also possible to calculate $NIR_V^{'}$ (radiance) as $NDVI \cdot NIR_T^{'}$, however, we only consider the reflectance case here. More specifically, $NDVI \cdot NIR_T$ serves as a reliable proxy of $\mathrm{BRF_V}$ in the NIR band ($\mathrm{NIR_V}$), which can be more succinctly expressed by combining Eq. 4 with Eq. 8:

$$\begin{aligned} NDVI \cdot NIR_T &\approx NIR_V \\ &\approx i_0 \cdot \omega_N \cdot f_N^{esc}. \end{aligned} \tag{9}$$

There are two important messages to take from Eqs. 8 and 9. First, $NDVI \cdot NIR_T$ is one possible approach for approximating $\mathrm{NIR_V}$. Intuitively, the approach works because both $\mathrm{NIR_T}$ and NDVI vary with soil brightness, but in an opposite manner: darker soils have a higher NDVI but lower $\mathrm{NIR_T}$, while brighter soils have a lower NDVI but higher $\mathrm{NIR_T}$ (Qi et al., 1994). As the fraction of vegetation cover approaches unity, NDVI also approaches unity and the product reduces to $\mathrm{NIR_T}$. Note that because NDVI does not necessarily span between 0 and 1, the approach underestimates the true value of $\mathrm{BRF_V}$(NIR) for high fractions of vegetation cover (Figure 1; though these effects can be further mitigated, see Discussion). Recognizing that there might exist alternative approaches for estimating $\mathrm{NIR_V}$, for purposes of both clarity and brevity, from this point forward we will refer to the product of NDVI and $\mathrm{NIR_T}$ as simply "$\mathrm{NIR_V}$." We will contrast this approximation against $\mathrm{BRF_V}$(NIR), which from this point will signify the true value of the BRF of vegetation.

Second, and more importantly for the derivation at hand, Eq. 9 suggests that $\mathrm{NIR_V}$ (as approximated by $NDVI \cdot NIR_T$) closely approximates the black soil condition imagined by Knyazikhin et al. (1998), providing a reliable proxy for estimating $\mathrm{BRF_V}$(NIR). The validity of this claim is immediately testable using SCOPE (van der Tol et al., 2009), which allows the simulation of canopy radiative transfer via an implementation of PROSAIL (Baret et al., 1994; Jacquemoud and Baret, 1990; Verhoef, 1984). Using SCOPE, we allowed solar and view angles, soil brightness, and canopy structure to vary randomly across their full valid ranges (Table 1). The

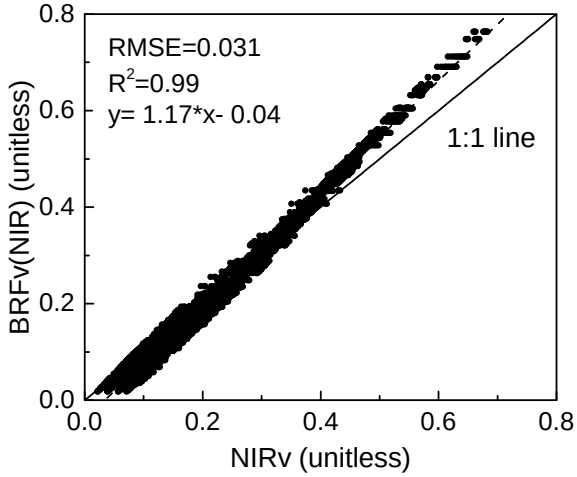

Figure 1: NIR_V closely approximates BRF_V, the vegetative component of pixel BRF, across a wide array of fractional vegetation cover, soil backgrounds, and leaf angle distributions. NIR_V underestimates low values of BRF_V and overestimates higher values of BRF_V. All values generated using SCOPE, with parameters drawn from ranges shown in Table 1.

R^2 between NIR_V and BRF_V exceeded 0.99 across 5,040 random combinations of input variables (Figure 1). By contrast, NIR_T shows wide dispersion against BRF_V at lower levels of vegetation cover, with gradual convergence of NIR_T and BRF_V as vegetation comprises a larger fraction of the scene (Figure S1).

2.3 Measuring f^{esc} remotely

Eq. 9 can then be rearranged to calculate the common term, f_N^{esc}, shared between NIR_V and SIF_N:

$$f_N^{esc} \approx \frac{NIR_V}{i_0 \cdot \omega_N}. \tag{10}$$

Using Eq. 10 in practice requires two additional assumptions. First, ω_N, the NIR leaf albedo, is relatively conservative both within and across species (Asner, 1998; Gates et al., 1965) and, for purposes of this derivation, we assume ω_N takes a constant value of 1. Second, calculating i_0 requires additional knowledge of canopy architecture, including the leaf projection function($G(\Omega)$; Ross 1981) and the clumping index (CI; Chen 1996). While both $G(\Omega)$ and CI are measurable quantities, both strongly vary in time and space, making them difficult to quantify remotely (Raabe et al., 2015; Ryu et al., 2010).

Instead, we make the further simplifying assumption that i_0 is approximated by canopy fPAR, the fraction of absorbed photosynthetically active radiation (PAR). PAR is strongly absorbed by plant canopies; leaf albedo within the visible range (ω_V) is small and, for our purposes, can be assumed to approach 0 (Gates et al., 1965). Following Stenberg et al. (2016) and assuming $\omega_V = 0$, we can explicitly relate i_0 to fPAR via canopy absorbance of visible light ($\mathrm{ABS_V}$):

$$\begin{aligned} fPAR &= ABS_V \\ &= i_0 \cdot \frac{1-\omega_V}{1-p\omega_V} \\ &\approx i_0. \end{aligned} \tag{11}$$

Here, p represents the probability of a photon recolliding with the canopy after its initial (non-absorbing) interaction with the canopy (see Appendix). For clarity, Eq. 11 treats the soil as black, ignoring the minor contribution of solar photons reflected by the soil that are ultimately absorbed by vegetation. This assumption, however, is not invoked at any point in our analysis, including the validation of Eq. 11 below. When evaluated using SCOPE, Eq. 11 holds across a wide array of conditions, where both LAI and FVC were varied (see Methods). For all combinations of LAI and FVC, fPAR is strongly correlated with i_0, having an the RMSE of 0.03, and an R^2 exceeding 0.99, demonstrating that fPAR closely approximates i_0 (Figure 2). Furthermore, while the assumption that $\omega_V = 0$ is useful for deriving the relationship between f^{esc} and $\mathrm{NIR_V}$, this assumption is not invoked in the radiative transfer simulations used to validate our approach. It is also worth pointing out that while NDVI (used to approximate $\mathrm{NIR_V}$) and fPAR are related to each other, their relationship is not strictly linear due to the fact that canopy architecture (e.g., leaf inclination angle, CI) has unequal effects on NDVI and fPAR (Figure S2).

Together with our assumption that $\omega_N = 1$, we can then rewrite Eq. 10 to read:

$$f_N^{esc} \approx \frac{NIR_\mathrm{V}}{fPAR}, \tag{12}$$

which is both computationally tractable and easily estimated from existing *in situ* and remote sensing measurements. A more detailed derivation relating f^{esc} of SIF to f^{esc} of NIR reflectance is presented in the Appendix.

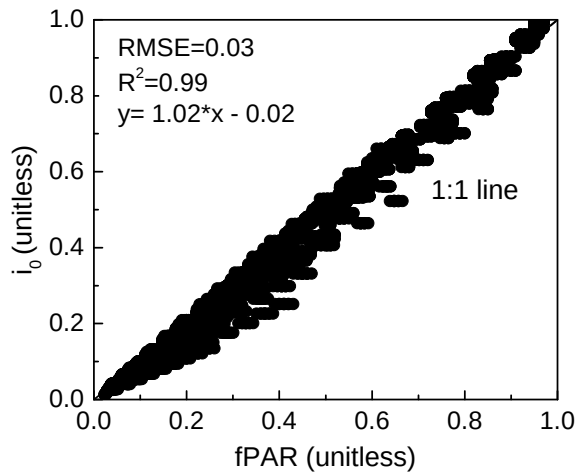

Figure 2: fPAR is a good approximation of canopy directional interceptance, i_0, across canopies with varying leaf area and fraction of vegetation cover. All values generated using SCOPE, with parameters drawn from ranges shown in Table 1.

3 Materials and Methods

3.1 Testing $\mathbf{NIR_V}$ as the basis for estimating f^{esc}

We evaluated Eq. 12 using both a one-dimensional (1-D) and a three-dimensional (3-D) radiative transfer model. Radiative transfer models enabled us to exhaustively test numerous parameters that affect f^{esc}, allowing for a more comprehensive evaluation of Eq. 12 than would be possible using *in situ* measurements alone. For both models, our general approach was to randomly vary key parameters that affect f^{esc}, including leaf-level spectral properties (e.g., chlorophyll content), leaf area index (LAI), leaf angle distribution (LAD), and soil brightness.

3.1.1 SCOPE: 1-D Radiative Transfer Simulations

We began our evaluation of Eq. 12 using the Soil Canopy Observation, Photochemistry and Energy (SCOPE) model, which is capable of simulating radiative transfer, energy balance, and photosynthesis, as well as the SIF of individual leaves within the canopy and total emitted SIF across the full spectrum of chlorophyll fluorescence (van der Tol et al., 2009). Using SCOPE, we conducted a set of simulations where we randomly varied parameters affecting both f^{esc} and scene NIR reflectance. In particular, we randomly varied leaf chlorophyll content (Cab), LAD, LAI, the reflectance profile of soil, view zenith angle, and solar zenith angle (Table 1). For each simulation, we compared simulated f^{esc} against f^{esc} as derived in Eq. 12, $\frac{NIR_V}{fPAR}$. For reference, we also com-

	Variable	Values
Canopy Structure	Leaf Area Index	[0.5, 1, 3, 5]
	Leaf Angle Distribution	Spherical, Erectophile, Planophile
Sun-Sensor Geometry	Solar Zenith Angle	[20, 30, 40, 50, 60]
	View Zenith Angle	[0, 10, 20, 30, 40, 50, 60]
Soil Background	Soil Spectra	Four soil spectrum
Leaf Spectral Properties	Leaf Chlorophyll Content (Cab)	[40, 60, 80]

Table 1: Parameters varied in SCOPE simulations. Default values for SCOPE v1.70 were used for all other parameters.

pared the NIR_V-based approach against the NIR_T approach proposed in Eq. 12 of Yang and van der Tol (2018), which specifies f^{esc} as:

$$f^{esc} = \frac{NIR_T}{\omega_N \cdot i_0}. \tag{13}$$

We further examined variations in FVC using a simple linear spectral mixture model, with the end members of i) vegetation, with values derived from SCOPE with an LAI of 3, and ii) bare soil. The spectral properties of each scenario were calculated by the area proportional to each end member, with FVC ranging between 0.1 and 1.

All SCOPE simulations were conducted using version 1.70 of the model. For each simulation, directional and total emitted SIF were extracted at 760 nm. NIR_V was calculated using red reflectance at 648 nm and NIR reflectance at 858 nm to be consistent with the red and NIR bands of the Moderate Resolution Imaging Spectroradiometer (MODIS) for future practical use, though it is worth noting that the NIR of vegetation has little variation from 760–900 nm (Gates et al., 1965). We used the SCOPE canopy gap fraction variable, $gap.Ps$, to calculate i_0 as $1 - gap.Ps$. Finally, we calculated BRF_V from SCOPE for each simulated condition by keeping all parameters equal, but inserting a black soil background.

3.1.2 DART: 3-D Radiative Transfer Simulations

We conducted a similar experiment testing the validity of Eq. 12 using the Discrete Anisotropic Radiative Transfer (DART) model (Gastellu-Etchegorry et al., 2004). DART allows the simulation of light within the optical domain and, due to recent developments described in Gastellu-

	Variable	Values
Canopy Structure	Leaf Area Index	2
Sun-Sensor Geometry	Solar Zenith Angle	30°
	View Zenith Angle	0°-70° with step of 5°
Soil Background	Soil Spectra	Three soil spectrum (Figure S3)
Leaf Spectral Properties	Leaf Chlorophyll Content	58

Table 2: Parameters varied in DART simulations. Default values were used for all other parameters.

Etchegorry et al. (2017), DART is also capable of modeling SIF. Unlike SCOPE, which operates under the assumption of a horizontally homogeneous canopy, DART provides a more realistic representation of partial vegetation cover. As a result, DART provides a useful tool for testing the relationship between $\mathrm{NIR_V}$ and $\mathrm{BRF_V}$ under conditions of sparse vegetation cover.

Due to the computational demands of DART, we focused our attention on varying soil properties and viewing geometry across DART runs. Leaf area, solar zenith angle, and chlorophyll content of the canopy were held constant across all runs (Table 2). We instead concentrated on varying soil brightness, using three separate soil spectra included in DART (Figure S3). 3-D renderings of the simulated canopy are included in the supplementary materials (Figure S4). DART directly calculates both red and NIR reflectance, from which we calculated $\mathrm{NIR_V}$. DART also simulates observed SIF ($\mathrm{SIF_{Obs}}$), but does not provide ready access to leaf-level estimates of SIF, meaning we were unable to calculate $\mathrm{SIF_{Total}}$ and f^{esc} of SIF.

Instead, we compared simulated $\mathrm{NIR_V}$ under various soil brightness conditions against $\mathrm{BRF_V}$, which we calculated by running a second set of DART simulations where the soil background was assumed to be black. These simulations allowed us to evaluate the performance of $\mathrm{NIR_V}$ and $\mathrm{NIR_T}$ for estimating $\mathrm{BRF_V}$, as outlined in Eq. 9. Recall that $\mathrm{BRF_V}$ comprises three parts: i_0, ω_N, and f^{esc}. As a result, the utility of $\mathrm{NIR_V}$ as a predictor of f^{esc} can be assessed by examining the linearity of $\mathrm{NIR_V}$-$\mathrm{BRF_V}$ relationship, when evaluating parameter combinations that mainly affect f^{esc}. Similarly, we directly evaluate the SIF-$\mathrm{NIR_T}$ and SIF-$\mathrm{NIR_V}$ relationship using data from the DART simulations. As with the SCOPE simulations, $\mathrm{SIF_{Obs}}$ was calculated at 760 nm, while $\mathrm{NIR_V}$ was calculated using reflectance red reflectance at 648 nm and NIR reflectance at 858 nm. For continuity with Yang and van der Tol (2018), $\mathrm{NIR_T}$ was calculated at 760 nm.

3.2 Empirical Evaluation of $\mathbf{NIR_V}$ compared to $\mathbf{NIR_T}$

We performed an empirical evaluation of NIR_V as the basis for estimating f^{esc} by directly comparing NIR_V against measurements of SIF. Such a comparison allowed empirical validation of the SIF-NIR_V relationship, with the goal of demonstrating that NIR_V does indeed approximate the "black soil" condition. Previously, Liu et al. (2018) and Yang and van der Tol (2018) proposed using NIR_T for estimating f^{esc}. However, both studies invoked the black soil assumption, assuming perfect absorption of solar photons by the soil background. Our derivation of f^{esc} and the simulation results that follow make no such assumption. Combining our model-based results with an empirical comparison of NIR_V and NIR_T offers a more comprehensive evaluation of how the differing approaches operate in practice.

We combined measurements of NIR_V and NIR_T from MODIS with near-infrared SIF retrievals from the newly launched TROPOMI sensor (Köhler et al., 2018). Specifically, the proposed joint dependency of SIF and NIR_V on i_0 and f_N^{esc} (as illustrated by Eq. 2) can be more simply expressed and evaluated by exploring the proportionality of SIF to NIR_V using actual remote sensing measurements:

$$SIF \propto NIR_V. \tag{14}$$

Black soil does not exist under real measurement conditions, meaning Eq. 14 can be directly contrasted against the proportionality of SIF to NIR_T:

$$SIF \propto NIR_T. \tag{15}$$

If NIR_T is sufficient for calculating f^{esc} in non-idealized situations, there should be no significant difference between the SIF-NIR_T and the SIF-NIR_V relationship. Such a comparison provides an empirical test of the differences of NIR_T and NIR_V in approximating the "black soil condition", as opposed to specifically testing various techniques for estimating f^{esc} that require additional inputs (e.g, the approach to estimating f^{esc} proposed by Yang and van der Tol (2018) requires i_0 as an input).

To perform the comparison, we selected five sites with various fractions of vegetation cover from across North America. We then extracted daily near-infrared SIF retrievals from the cloud

filtered and globally gridded TROPOMI SIF dataset described by Köhler et al. (2018), which has a spatial resolution of 0.2°. We combined SIF data with daily NIR_V and NIR_T observations from the nadir-corrected MODIS reflectance product MCD43A4v6 regridded to 0.2° (Schaaf et al., 2002). MODIS data were used, rather than radiances from TROPOMI because atmospherically corrected TROPOMI radiance data at the necessary wavelengths are not presently available. This introduces angular differences between the TROPOMI and MODIS data, though such discrepancies do not influence the inference derived from comparing SIF against NIR_T and NIR_V. Furthermore, the majority of TROPOMI SIF retrievals have a phase angle that falls between 20° and 60° (Köhler et al., 2018), while the MODIS data has been adjusted to nadir. These two facts combine to mitigate the severity of the disagreement between SIF and reflectance measurements that are solely attributable to viewing geometry. To facilitate comparison between flux measurements of SIF and unitless measurements of reflectance, we normalized SIF observations by at-sensor solar radiance. This ensured that the observed SIF-NIR relationships were not driven by an underlying PAR-NIR relationship. Together, these data allow direct evaluation of Eqs. 14 and 15. MODIS data were processed using the Google Earth Engine Python API. TROPOMI data were downloaded from ftp://fluo.gps.caltech.edu/data/tropomi/.

3.3 Correcting Virtual Satellite Retreivals

Finally, we used SCOPE to construct a virtual experiment to demonstrate the practical utility of using NIR_V-derived estimates of f^{esc} to estimate SIF_{Total} from directional-dependent simulations of SIF_{Obs}. In recent years, SIF has emerged as a useful remote measurement of APAR (Du et al., 2017; Yang et al., 2018) and GPP (Frankenberg et al., 2011b; Guanter et al., 2014; Smith et al., 2018; Sun et al., 2017; Yang et al., 2015; Zhang et al., 2016) at scales ranging from individual study sites to the globe. Many of these studies, however, rely on using fixed scaling factors between SIF_{Obs} and the variable of interest. These scaling factors, however, often ignore variations in f^{esc} that affect the value of SIF_{Obs}. Failure to account for f^{esc} makes it difficult to study variations in Φ_F at the global scale and potentially influences the interpretation of canopy- and global-scale relationships between SIF, GPP, and APAR.

To demonstrate this effect and explore the usefulness of Eq. 12 for calculating SIF_{Total} from measurements of SIF_{Obs}, we extracted solar and viewing geometry data from the Global Ozone Monitoring Experiment–2 sensor (GOME-2; a widely used SIF sensor) for a single location. This

allowed us to vary the solar and view angle parameters in SCOPE to match local conditions, as if the site were viewed by GOME-2 (Table 3). We then calculated the relative error introduced in calculating SIF_{Total} from SIF_{Obs} using NIR_V and Eq. 12. We also evaluated the relative error of assuming that any one value of SIF_{Obs} has a constant scaling with SIF_{Total} and the relative error in estimating SIF_{Total} from NIR_T-derived estimates of f^{esc}, following the approach of Yang and van der Tol (2018) (Eq. 13). Along with varying solar angle and view angle, we also simulated various values of FVC ranging from 0.1 to 1.

	Variables	Values
Canopy Structure	Leaf Area Index	3.7
	Leaf Angle Distribution	Erectophile
	Fractional Vegetation Cover	0.3–1
Sun-Sensor Geometry	Solar Zenith Angle	26.3°–36.4°
	View Zenith Angle	0.9°–33.6°

Table 3: Critical parameters for the virtual experiment testing the usefulness of NIR_V to calculate SIF_{Total} from SIF_{Obs}. Realistic solar and view angles were extracted from actual GOME-2 observations for a single location at 38.2013N, 127.2506E.

4 Results

4.1 SCOPE Simulations of f^{esc}

Eq. 12 states that the ratio of NIR_V and fPAR approximates the canopy escape ratio. To validate this formulation, we began by running two simple simulations in SCOPE: while holding leaf albedo constant and LAI at 3, we varied canopy leaf angle between erectophile (lower escape ratio) and spherical (higher escape ratio) (Figure 3). fPAR varied by less than 8% across the two simulations, while the NIR_V of the two canopies changed by 58.1% (Figure 3A). f^{esc} across the two simulations differed by 54.3%, which is roughly proportional to the differences in the ratio of NIR_V to fPAR between the spherical and the erectophile canopies (Figure 3B). Previous empirical work investigating the relationship of NIR_V and fPAR at eddy covariance sites on a per biome basis found similar results: canopies of widely varying architecture (e.g., with both different f^{esc} and NIR_V), tended to have similar values of fPAR (Badgley et al., 2017). Figure 3 emphasizes that canopies can have similar values of fPAR, while having considerably different values of NIR_V

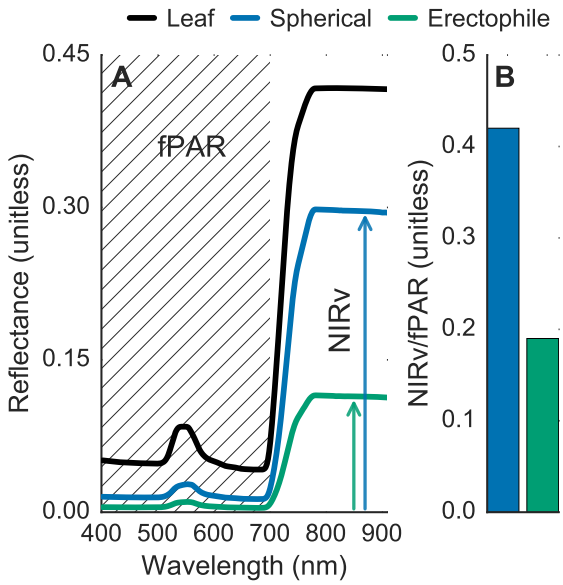

Figure 3: Canopies with different architectures can have similar values of fPAR, but significantly different values of $\mathbf{NIR_V}$ and f^{esc}. Changes in leaf angle distribution cause subtle changes in fPAR but large changes in NIR_V, making the ratio of NIR_V and fPAR a useful index of f^{esc}. All data from SCOPE, with LAI held constant at 3 and fixed leaf spectral properties (black). Data generated using SCOPE v1.70.

and f^{esc}. Any change in LAD causes changes in both fPAR and NIR_V. Yet because canopies so strongly absorb visible light ($\omega_V \approx 0$) and fPAR is strongly determined by total leaf area, changes in fPAR are relatively minor. NIR, however, is strongly scattered by leaves ($\omega_N \approx 1$), meaning even small deviations in sun-canopy-sensor geometry yield large changes in NIR_V that are proportional to the fraction of NIR photons, whether reflected or fluoresced, capable of escaping the canopy.

We found that the ratio of NIR_V to fPAR closely approximated f^{esc} across a wide array of simulated conditions, whereby Cab, LAD, LAI, soil NDVI, and both solar and view geometry varied (Figure 4). As predicted by Eq. 12, $\frac{NIR_V}{fPAR}$ is strongly linear with f^{esc}, having an R^2 of 0.91, RMSE of 1.48%, and average relative error (ARE) of 7.3%. Furthermore, the slope of $\frac{NIR_V}{fPAR}$ against the true, simulated value of f^{esc} is close to one, with only a small, positive intercept. By comparison, the NIR_T-based estimation of f^{esc} systematically overestimated f^{esc}, with an R^2 of 0.11, RMSE of 9.41%, and ARE of 45.2%. While $\frac{NIR_T}{i_0 \cdot \omega_N}$ is linear with f^{esc} for any given soil background, variations in soil reflectance introduce a large and variable intercept in the NIR_T-f^{esc} relationship, rendering NIR_T-based estimates of f^{esc} highly uncertain. The underlying NIR_T-f^{esc}

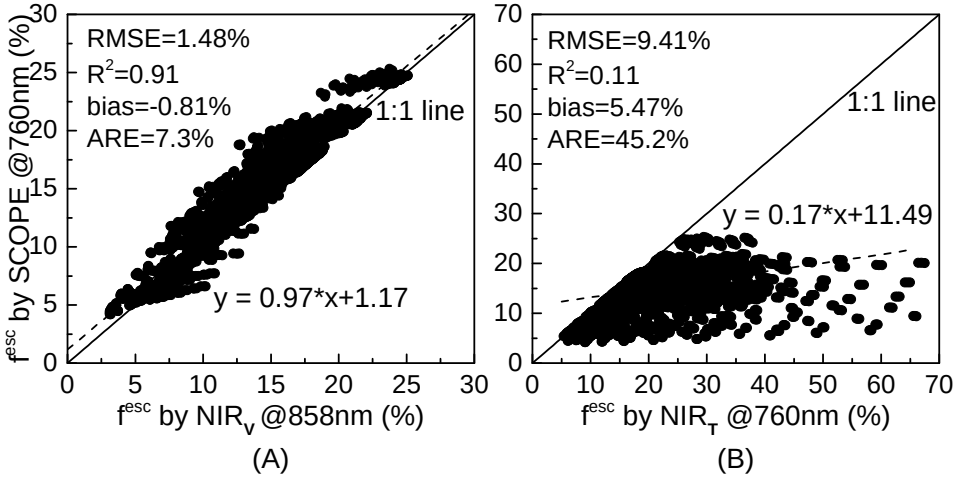

Figure 4: A) The ratio of $\mathbf{NIR_V}$ to fPAR closely approximates $\boldsymbol{f^{esc}}$, while B) f^{esc} calculated as $\frac{NIR_T}{i_0 \cdot \omega_N}$, following Yang and van der Tol (2018), is largely unrelated to modeled $\boldsymbol{f^{esc}}$ across the same range of conditions. All data produced using SCOPE, varying LAD, LAI, soil NDVI, view zenith angle, and solar zenith angle at random.

relationship, without taking into account i_0 and ω_N, exhibits a similar degree of non-linearity due to the effects of soil contamination (Figure S5). By accounting for variations in soil reflectance, $\mathrm{NIR_V}$ enables robust estimation of f^{esc} across the full range of expected observation conditions and with no need for additional information about soil reflective properties.

4.2 DART Simulations of $\mathrm{BRF_V}$

A second set of simulations using the 3-D radiative transfer model DART demonstrates the generality of the $\mathrm{NIR_V}$-$\mathrm{BRF_V}$ relationship when more realistic radiative transfer processes are taken into account (Figure 5). Because DART does not generate per-leaf estimates of SIF, we instead evaluated the suitability of $\mathrm{NIR_V}$ as the basis for estimating f^{esc} by comparing $\mathrm{NIR_V}$ and $\mathrm{NIR_T}$ against $\mathrm{BRF_V}$, following Eq. 9. While soil brightness does introduce a bias into the estimation of $\mathrm{BRF_V}$ by $\mathrm{NIR_V}$, the $\mathrm{NIR_V}$-$\mathrm{BRF_V}$ relationship has a small RMSE of 0.026, a near-zero intercept, and a slope of 0.89 (Figure 5A). Variations in soil background result in a weaker relationship between $\mathrm{NIR_T}$ and $\mathrm{BRF_V}$ (Figure 5B). As found in the SCOPE simulations, $\mathrm{NIR_T}$ is mostly linear with $\mathrm{BRF_V}$ for any given soil brightness. However, variations in the soil background degrade the overall proportionality of $\mathrm{NIR_T}$ to $\mathrm{BRF_V}$, resulting in a RMSE of 0.107, an intercept of 0.11, and a slope of 0.4. As a result, using $\mathrm{NIR_T}$ to derive f^{esc} would require *a priori* information about soil spectral properties (to account for the influence of $\mathrm{NIR_S}$, see Eq. 5). $\mathrm{NIR_V}$ has a more ro-

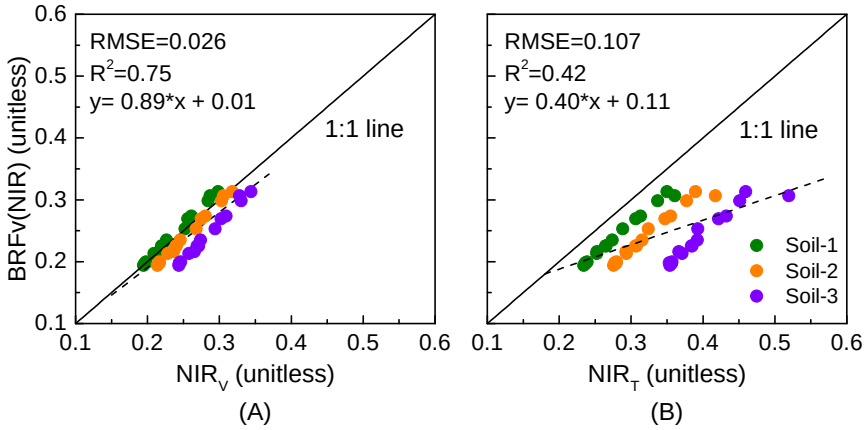

Figure 5: 3-D radiative transfer simulations of the A) NIR_V-BRF_V and B) NIR_T-BRF_V relationships from DART. NIR_V is strongly linear with BRF_V across varying soil backgrounds, demonstrating the usefulness of NIR_V as the basis for estimating f^{esc}, regardless of vegetation density.

bust relationship BRF_V and f^{esc} that does not require explicit consideration of soil background reflectance.

NIR_V also had a more consistent relationship with DART simulations of SIF_{Obs}, when compared to NIR_T (Figure 6). The SIF-NIR_V relationship has a small RMSE of 0.004 and a near-zero intercept of 0.01. Intriguingly, the SIF-NIR_T relationship is substantially stronger ($R^2 = 0.85$) than the NIR_T-BRF_V ($R^2 = 0.42$) relationship shown in Figure 5. This seemingly contradictory result has to do with the fact that for a discontinuous canopy backed by a bright soil background, accurately estimating f^{esc} of SIF requires consideration of the interaction of SIF photons with the soil background (BRF_M from Eq. 3). Under these conditions, BRF_M strongly contributes to the fraction of SIF photons that ultimately escape the canopy. In the case of a mostly uniform (e.g., BRF_S is small due to the spatial distribution of vegetation relative to the soil background, Figure S4), albeit discontinuous canopy, both NIR_V and NIR_T are capable of capturing the contribution of BRF_M to f^{esc}. However, NIR_V has still has a stronger relationship with SIF because it is less affected by BRF_S. As a result, following Eqs. 14 and 15, NIR_V offers a more robust starting point for estimating f^{esc} of SIF. Finally, Figure 6 can be thought of as a best-case scenario for the performance of NIR_T over a discontinuous canopy. As the canopy becomes less uniform (e.g., clumped in space) and BRF_S increases, the insensitivity of NIR_V to the soil background results in the SIF-NIR_V relationship remaining strongly linear ($R^2 = 0.83$), while the SIF-NIR_T relationship rapidly weakens and becomes non-linear ($R^2 = 0.62$; Figure S6).

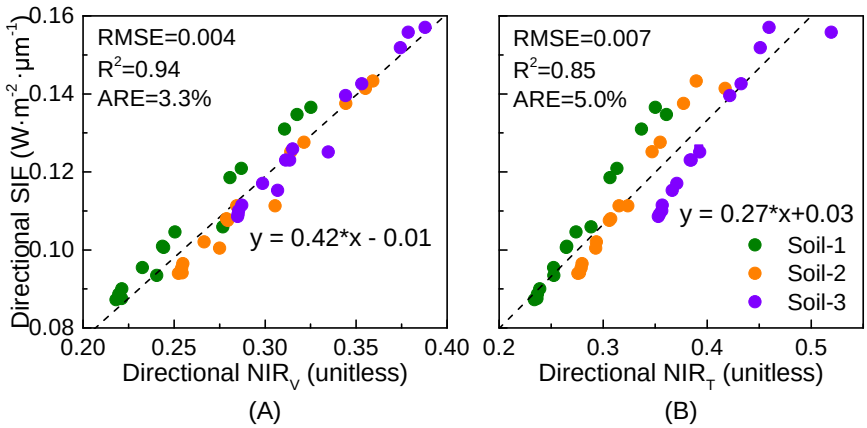

Figure 6: 3-D radiative transfer simulations of the A) SIF-NIR_V and the B) SIF-NIR_T relationship from DART. NIR_V is less sensitive to variation in the soil background and has a stronger linear relationship with simulated SIF. Reflectance profiles of each soil are provided in Figure S3.

4.3 Empirical Differences between NIR_V and NIR_T

Satellite measurements of NIR_V and SIF confirmed that NIR_V minimizes the effects of variation in soil background, whereas the SIF-NIR_T relationship is highly non-linear for sparse vegetation types (Table 4; see Figure S7 for individual site scatter plots). These data represent a direct test of Eqs. 14 and 15, as NIR_V and NIR_T must be proportional to SIF if either measurement is to be useful as the basis for estimating f^{esc} (Eq. 2). For each site, we calculated the difference in the coefficient of determination (R^2) between radiation normalized SIF, NIR_V, and NIR_T. While NIR_T and radiation normalized SIF show strong agreement over dense, continuous canopies, like crops and broadleaf forests (ΔR_2 = -0.01 and 0.11, respectively), the relationship is considerably weaker over sparse vegetation canopies. For biomes like sparse woodlands, NIR_V has a substantially stronger and more linear relationship with radiation normalized SIF than NIR_T (ΔR^2 = 0.53), though the SIF-NIR_V relationship did break down at the grassland site. Interestingly, NIR_V even outperformed NIR_T at US-Ha1 (Harvard Forest), a dense, mostly closed canopy deciduous broadleaf forest where soil contamination is expected to be minimal.

However, early in the season, before leaf flush, soil is readily visible from the satellite perspective, which causes a divergence in NIR_T from measured SIF (Figure S7). Thus, even though NIR_T is highly correlated with SIF for parts of the season, NIR_V has a more consistent, inter-seasonal relationship with SIF. Taken together, these results nicely illustrate that NIR_V, as defined in Eq.

9, does a better job of approximating the "black soil condition", whereas soil contamination renders NIR_T a less suitable candidate as the basis for calculating f^{esc}. NIR_V also outperforms the SIF-NDVI relationship at these sites, further demonstrating the utility of combining NDVI and NIR_T together (Figure S7).

Site (Ameriflux Code)	Lat./Lon.	Biome	SIF-NIR_V R^2	SIF-NIR_T R^2	ΔR^2 (NIR_V – NIR_T)
US-Ha1	42.52, -72.17	Broadleaf Forest	0.72	0.61	0.11
US-CZ1	37.109, -119.73	Oak/Pine Woodland	0.71	0.18	0.53
US-SCg	33.74, -117.69	Grassland	0.24	0.02	0.22
US-Ho1	45.20, -68.74	Evergreen Forest	0.70	0.16	0.54
US-Ne1	41.17, -96.47	Cropland	0.87	0.88	-0.01

Table 4: NIR_V has a stronger, more consistent relationship with daily measurements of SIF than NIR_T across multiple biomes. Daily MODIS reflectance values were compared against daily, at-sensor radiance normalized SIF measurements from the TROPOMI sensor for the period spanning March to August 2018.

4.4 Correcting Virtual Satellite Retrievals

Accurate estimates of f^{esc} allow the conversion of directional measurements of SIF_{Obs} into estimates of total emitted SIF, SIF_{Total}. Changes in both solar and viewing geometry cause variations in SIF_{Obs} that are unrelated to differences in the true value of total emitted SIF. Ideally, SIF_{Obs} should be converted to SIF_{Total} to serve as a common basis of estimating canopy APAR and, potentially, gross primary production. When we ran SCOPE using view angles taken from actual GOME-2 satellite retrievals for a single site, variations in viewing geometry resulted in upwards of 70% variation in SIF_{Obs} (Figure 7A). Naively relating any one value of SIF_{Obs} to total emitted SIF yielded a ±30% relative error in estimated SIF_{Total} (Figure 7B). Such variations have no direct link to physiology and, if not accounted for, significantly bias attempts to use SIF to infer canopy-scale and leaf-level physiology (e.g., Φ_F), especially across canopies with dissimilar architectures. By contrast, SIF_{Total} calculated from NIR_V-derived estimates of f^{esc} has a maximum relative error of ±4.9% and ARE of 2.2% (Figure 7C). Such minimal errors should allow SIF measurements to be more accurately compared across space and time to draw physiological inferences.

NIR_V provides a robust estimate of f^{esc} across all values of FVC, resulting in accurate estimation of SIF_{Total} even under sparsely vegetated conditions (Figure 8). NIT_T, on the on the

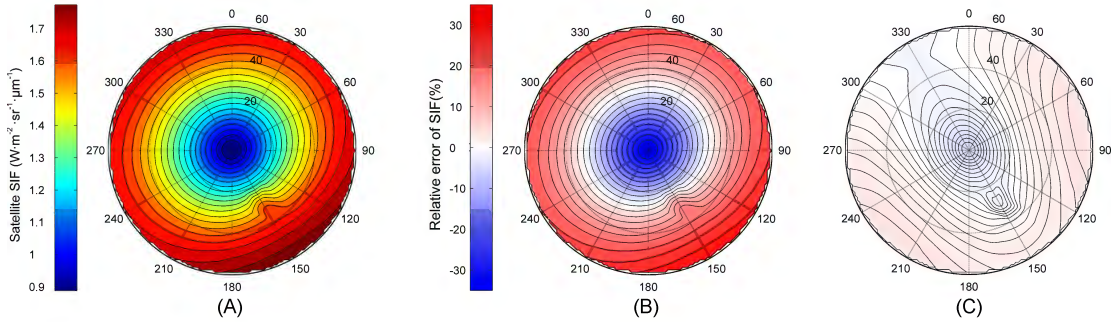

Figure 7: Variation in solar angle and view angle cause large differences in $\mathbf{SIF_{Obs}}$. A) View geometry alone causes upwards of a 70% difference in directional SIF, B) which if used as a proxy for total emitted SIF causes ±30% differences in estimated SIF_{Total}. C) Adjusting SIF by NIR_V-derived f^{esc} results in low relative errors of estimated SIF_{Total}. All data calculated using SCOPE, with FVC equal to 0.5.

other hand, is strongly affected by soil reflectance, resulting in errors exceeding 50% in estimated SIF_{Total} for low values of FVC. It is only under relatively high values of FVC (e.g., greater than 0.8) that NIR_T-derived estimates of SIF_{Total} are on average more accurate than estimates of SIF_{Obs} alone. The average relative error of directly scaling any one directional value of SIF_{Obs} to SIF_{Total} remains constant at roughly 20% across all simulated values of FVC because SIF is not influenced by soil background reflectance. Average relative error of NIR_V-based estimates of SIF_{Total} falls well below 10% for all values of FVC examined. Interestingly, the average relative error of NIR_V-based SIF_{Total} was lower than NIR_T-based estimates for all values of FVC, including when FVC reached unity. This result demonstrates the usefulness of NIR_V for both sparsely and densely vegetated scenes.

5 Discussion

We demonstrated that the ratio of NIR_V to fPAR is an accurate approximation of the escape ratio of near-infrared SIF photons, providing a theoretically-grounded and computationally tractable approach for translating directional-based SIF measurements to comparable, whole-canopy estimates of total emitted SIF. Importantly, the approach requires minimal assumptions and can be calculated using widely available optical remote sensing data. Our approach is immediately applicable to *in situ* studies of SIF and a wide range of satellite-based SIF platforms, including the newly launched TROPOMI sensor (Veefkind et al., 2012) and the upcoming FLEX mission (Drusch et

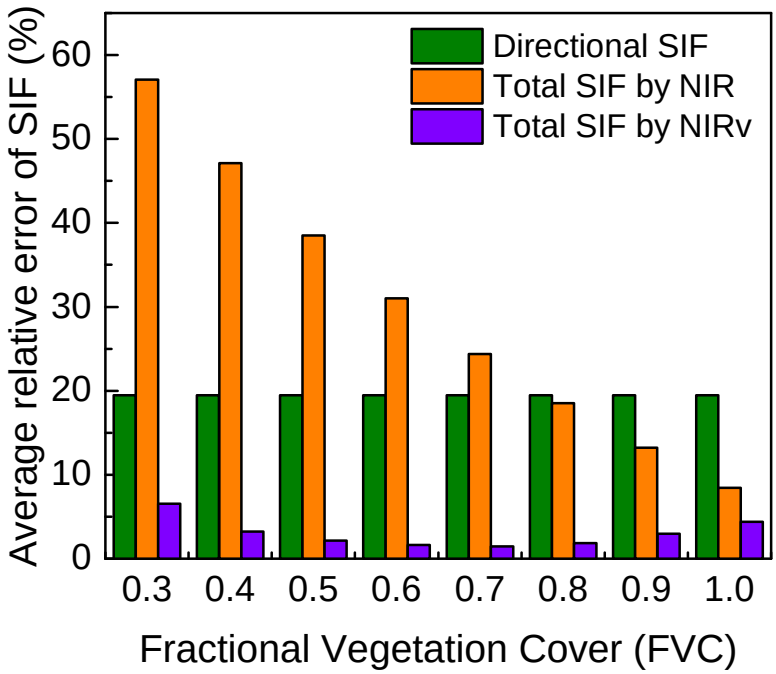

Figure 8: $\mathbf{SIF_{Total}}$, as estimated using f^{esc} derived from $\mathbf{NIR_V}$, has a lower relative error than both $\mathbf{SIF_{Total}}$ estimated from assuming a constant scaling between directional SIF and $\mathbf{SIF_{Total}}$ (green) and $\mathbf{SIF_{Total}}$ derived from $\mathbf{NIR_T}$-based estimates of f^{esc} (orange). All data simulated using SCOPE, with critical parameters outlined in Table 3.

al., 2017), both of which have access to simultaneous or near simultaneous measurements of reflectance and SIF, which allows for per-sounding f^{esc} adjustments by $\mathrm{NIR_V}$. Our approach is also useful for *in situ* studies of SIF, where diurnal shifts in sun-sensor geometry can significantly influence $\mathrm{SIF_{Obs}}$ and obscure underlying physiologyical changes in Φ_F (Figure 7). To date, there have only been a handful of studies explicitly focused on the escape ratio of SIF, including attempts to correct for it. Romero et al. (2018) proposed an approach based on canopy reflectance, transmittance, and soil reflectance to estimate the spectral shape of SIF emitted at the leaf-level. While useful, the dependence on prior knowledge of soil reflectance and canopy transmitance limits the practical application of the approach. Liu et al. (2018) took a purely statistical approach, combining machine learning with reflectance-based inputs to infer f^{esc} of both red and near-infrared SIF. While their approach performed well for even low LAI values, the approach we propose here using $\frac{NIR_V}{fPAR}$ is both mechanistically and computationally simpler. In an independent study, Yang and van der Tol (2018) showed that $\frac{NIR_T}{i_0 \cdot \omega_N}$ was a good approximation f^{esc} under the black soil condition. Our work directly extends this concept by demonstrating that $\mathrm{NIR_V}$ closely approximates the black soil condition and is readily applicable in real-world remote sensing applications (Table 4).

5.1 Canopy Spectral Invariants

Our approach builds on recent advances in canopy radiative transfer theory, especially the development of spectral invariant properties (SIP; Huang et al. 2007; Knyazikhin et al. 2013; Stenberg et al. 2016). SIP dramatically reduce the complexity of characterizing whole-canopy radiative processes, breaking down the radiative transfer process into three main components: i_0, the probability a photon interacts with vegetation; ρ_n, the probability a photon escapes the canopy on its n-th collision; and p_n, the probability a photon, after its n-th recollision, recollides with vegetation yet again. Together, i_0, ρ, and p can be combined to characterize even the most complex radiative environments, across all wavelengths of light. In many ways, the development of SIP is akin to the development of leaf-level spectral models, whereby detailed knowledge of the internal complexity of the leaf (e.g., chlorophyll content, mesophyll density) and its effect on radiative transfer, can instead be characterized by only a few parameters (e.g., Jacquemoud and Baret 1990). SIP enables the same reduction in complexity at the scale of the entire canopy (Stenberg et al., 2016).

Our results demonstrate that $\mathrm{NIR_V}$ serves as a new tool for capturing SIP parameters from

remote sensing. Indeed, the term f^{esc} can be explicitly expressed in terms of both ρ and p (see Appendix). Given that $\mathrm{NIR_V}$ also relates to i_0 (Eq. 9), $\mathrm{NIR_V}$ can in principle serve as the basis for individually retrieving i_0, ρ, and p. Fully separating the influence of each parameter, however, likely requires use of multi-angular data and perhaps some ancillary data (e.g., fPAR, leaf spectral properties). In the meantime, the fact that $\mathrm{NIR_V}$ captures the effects of i_0, ρ, and p is sufficient for accurately characterizing the canopy radiative environment and estimating $\mathrm{SIF_{Total}}$ from measurements of $\mathrm{SIF_{Obs}}$. Our formulation of using $\mathrm{NIR_V}$ to calculate f^{esc} might also find use in process-based ecosystem models, by way of simplifying canopy radiative transfer processes. Many of these models already simulate or take as inputs all the variables needed to estimate f^{esc} from $\mathrm{NIR_V}$. One potential use of these data suggested by our analysis would be explicitly scaling modeled estimates of $\mathrm{SIF_{Total}}$ to estimates of $\mathrm{SIF_{Obs}}$ for comparison with ground-based and satellite observations of SIF. Finally, $\mathrm{NIR_V}$ has the distinct advantage of approximating black soil conditions, meaning it is readily usable in remote sensing applications, where LAI and FVC are often low and soil contamination is nearly universal (Figure 4; Table 4). Previously proposed SIP-based indices, like the directional area scattering factor (DASF), require explicit consideration of soil background effects (Knyazikhin et al., 2013). In fact, $\mathrm{NIR_V}$ and its relationship to SIF and $\mathrm{BRF_V}$ can be expressed in terms of DASF (see Appendix, Eq. A9), providing additional opportunities for the synthesis of $\mathrm{NIR_V}$, SIP, and global scale remote sensing of vegetation (Köhler et al., 2018). Such synthesis should help resolve outstanding questions about the relative controls of canopy-scale structure and physiology on plant productivity, a topic that has received growing attention in recent years (e.g., Migliavacca et al., 2017).

5.2 The Radiative Transfer of Fluorescence

Calculating total emitted near-infrared SIF, as opposed to directional SIF, is an important step in using SIF to accurately estimate GPP. Several recent SIF studies, including Guanter et al. (2012), Zhang et al. (2016), and Sun et al. (2018) found that the slope of the SIF-GPP relationship varied by biome. However, these studies did not fully account for directional effects and canopy escape ratio. As a result, the per biome relationships previously described might be partly caused by differences in latitude and time of year, LAD, FVC, LAI and soil brightness affecting f^{esc}. Although the SIF-GPP relationship can be influenced by many factors, including physiological (e.g., C3 and C4 pathways of photosynthesis) and environmental factors, variations in the radiative transfer of

SIF (manifest in differing f^{esc}) can result in ±30% differences in observed SIF (Figure 7), which likely plays an important role in explaining spatial patterns of SIF at the global scale.

Accurate estimation of $\mathrm{SIF_{Total}}$ is especially critical to efforts to study variations in fluorescence yield (Φ_F, see Eq. 1) at the canopy scale and beyond. Φ_F is itself directly related to how energy is partitioned between photochemical and non-photochemical processes within the leaf, making the measurement and prediction of Φ_F an essential step in successfully using SIF to investigate plant physiology (Porcar-Castell et al., 2014). However, Φ_F is both a small (approx. 1% ± 0.5% of APAR) and highly dynamic signal (Krause and Weis, 1991), varying on daily and seasonal timescales (Miao et al., 2018; Porcar-Castell, 2011; Yang et al., 2018), as well as across space (Atherton et al., 2017; Malenovský et al., 2009). Such a small, complex signal, whose variations are small relative to its mean value, is easily obscured by f^{esc} induced variations in SIF. $\mathrm{NIR_V}$ offers one approach for removing the effects of f^{esc}, which is a key step in the challenge of mechanistically linking SIF to GPP. Previously, Badgley et al. (2017) used simulations to show that the ratio of SIF to $\mathrm{NIR_V}$ can be used to discern variations in Φ_F. Our results relating $\mathrm{NIR_V}$ to f^{esc} provide a physical explanation for why this approach works by linking $\mathrm{NIR_V}$ to $\mathrm{BRF_V}$.

In evaluating the suitability of using $\mathrm{NIR_V}$ to estimate f^{esc} of SIF, it is helpful to consider uncertainties in our approach. From a physical standpoint, SIF and $\mathrm{NIR_V}$ are generated by different processes within the canopy, which means that canopy-scale f^{esc} of SIF can differ from the f^{esc} of $\mathrm{NIR_V}$. More specifically, vertical variations and differences in Φ_F and ω_N cause SIF and NIR photons to originate from different places within the canopy. Thankfully, these differences are small, as demonstrated by a series of supplementary SCOPE simulations we conducted to quantify the effect (Table S1). We ran three simulations: i) a baseline for comparison, ii) a simulation where we varied meteorological and biochemical parameters that affect Φ_F but have no influence on ω_N, and iii) a simulation where we varied leaf optical parameters affecting ω_N but have no influence on Φ_F. In both instances, varying meteorological variables and leaf optical properties causes only the slightest change in the R^2 and RMSE of the f^{esc} of SIF and f^{esc} of $\mathrm{NIR_V}$ relationship, (Figure S8).

One additional uncertainty in our approach concerns the spectral mismatch between near-infrared SIF (calculated between 740–760 nm) and $\mathrm{NIR_V}$, measured at 858 nm to be consistent with MODIS. Differences in leaf albedo across these wavelengths mean that the f^{esc} of a solar photon at 858 nm is not strictly equal to the f^{esc} of a SIF photon at a shorter wavelength. In

practice, however, these differences are small. Using SCOPE, we performed two additional simulations: i) simulating both NIR_V and SIF at 760 nm and ii) simulating SIF at 740 nm and NIR_V at 858 nm. As expected, measuring NIR_V and SIF at the same wavelength improves the linearity of f^{esc} estimated by NIR_V with simulated f^{esc} of SIF ($R^2 = 0.93$, up from 0.91; Figure S9). In practical terms, however, NIR reflectance is typically measured at much longer wavelengths to avoid several strong atmospheric absorption features that complicate the accurate retrieval of surface reflectance from space-borne sensors. MODIS, VIIRS (the Visible Infrared Imaging Radiometer Suite), and Landsat all measure NIR at wavelengths extending beyond 800 nm. Therefore, from a data availability standpoint, satellite-based studies that use NIR_V from these sensors likely necessitate accommodating some degree of spectral mismatch when compared against SIF. However, studies should consider calculating f^{esc} using the same wavelength as retrieved fluorescence if the NIR data is available. In the same way, SIF measured at 740 nm, where chlorophyll more strongly reabsorbs SIF photons, degrades the accuracy of NIR_V-derived f^{esc} (Figure S10). While this effect is small, causing an increase of RMSE of less than 0.2% and a reduction of R^2 of 0.08, it is nonetheless worth mentioning. Future work to more accurately characterize the within-canopy re-absorption of SIF (e.g., Romero et al., 2018) and incorporate such effects into SIF retrievals can help ameliorate the uncertainties that arise from the spectral mismatch of SIF and NIR_V.

5.3 Approximating BRF_V with NIR_V

NIR_V minimizes the effects of variations in soil brightness, even under conditions where the NDVI of the soil is high and LAI (or FVC) is low (Figure 4). Yet in these cases, it is important to keep in mind that NIR_V is still only an approximation of BRF_V. In our simulations, NIR_V was slightly lower than BRF_V when the LAI was low and, by contrast, was higher than BRF_V when the LAI was high (Figure 1). This is due to the fact that NDVI is not strictly equal to 0 when LAI is 0 and does not necessarily equal 1 when LAI is high because non-vegetated surfaces (e.g., soil) can have a non-zero NDVI and FVC rarely reaches 1.

In practical terms, this effect can be further reduced by normalizing NDVI on a per-pixel basis to account for spatial variation in the multi-year average value of $NDVI_{min}$ and $NDVI_{max}$. More specifically, the NDVI in Eq. 8 could instead be replaced by $NDVI'$, which takes the form:

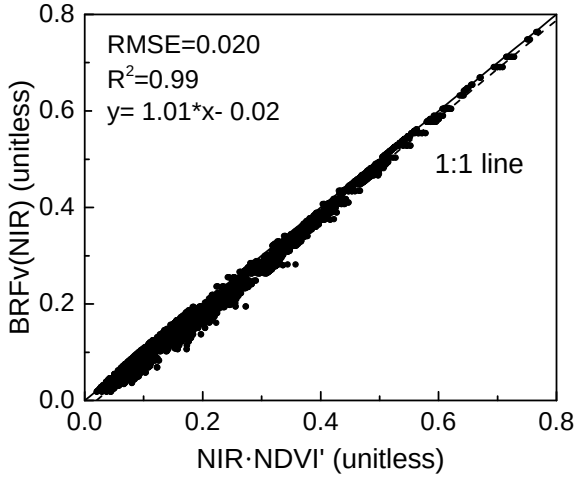

Figure 9: $\mathbf{NIR_V}$ can be further improved by accounting for per-pixel minimum ($\mathbf{NDVI_{min}}$) and maximum ($\mathbf{NDVI_{max}}$) values of NDVI. $\mathrm{NDVI_{min}}$ and $\mathrm{NDVI_{max}}$ can be derived from multi-angular remote sensing data, allowing $\mathrm{NIR_V}$ to even more closely approximate $\mathrm{BRF_V}$ (see Eq. 9).

$$NDVI^{'} = \frac{NDVI - NDVI_{min}}{NDVI_{max} - NDVI_{min}}. \tag{16}$$

In initial simulations where Eq. 16 is substituted into Eq. 8, we found a 35% reduction in RMSE of the $\mathrm{NIR_V}$-$\mathrm{BRF_V}$ relationship, with especially large improvements under extremely high and low values of LAI and FVC (Figure 9). Adjusting for the overall range of NDVI makes the $\mathrm{NIR_V}$-$\mathrm{BRF_V}$ relationship nearly one-to-one, with a small intercept of 0.02 and a slope of 1.01.

Fully adopting Eq. 16 would introduce two additional unknown parameters, $\mathrm{NDVI_{min}}$ and $\mathrm{NDVI_{max}}$, which might hinder application. However, there exist multi-angular remote sensing approaches for quantifying $\mathrm{NDVI_{min}}$ and $\mathrm{NDVI_{max}}$ that could lead to further improvements in $\mathrm{NIR_V}$, especially over sparse canopies (Mu et al., 2017; Song et al., 2017). Our analysis of MODIS and TROPOMI data showed that the $\mathrm{NIR_V}$-SIF relationship was relatively non-linear at a sparsely vegetated grassland site, which might arise from $\mathrm{NIR_V}$ being an inadequate approximation of the black soil condition when vegetation cover is extremely low (Table 4 and Fig. S7). Future work will need to establish the exact lower bound of FVC where the $\mathrm{NIR_V}$ approximation of $NDVI \cdot NIR_T$ breaks down in practice. Further improvements could also be made by properly accounting for spatial and temporal variation in ω_N, the leaf single scattering albedo in the NIR band (see Eq. 4). Such a modification would introduce yet another per-pixel parameter, though

accounting for variations in ω_N might prove practical for site-level studies.

5.4 Applications without knowledge of fPAR

Perhaps the largest downside to our proposed measure of f^{esc} is its reliance on readily available and reliable fPAR data. In fact, using Eq. 12 to estimate total emitted SIF not only requires fPAR, it also requires that $\mathrm{NIR_V}$ be calculated with near-identical sun-canopy-sensor geometry to SIF. The forthcoming FLEX mission, for example, will fly in tandem with another European satellite, Sentinel 3 (S-3), allowing the co-registration of a FLEX-based SIF product with the S-3 fPAR product (Gobron, 2010) and $\mathrm{NIR_V}$, as laid out in the FLEX mission concept plan (Drusch et al., 2017). Development of fPAR products based on data from existing SIF sensors that also make reflectance measurements in the visible domain (such as GOME-2), could provide another avenue for using our $\mathrm{NIR_V}$-based correction of f^{esc}. Further complications are introduced by the need to measure $\mathrm{fPAR_{green}}$, as opposed to simply the interaction of photons with non-photosynthetic aspects of the canopy. This is a lingering challenge that continues to motivate advances in the remote sensing of fPAR (e.g., Zhang et al., 2005) that will ultimately benefit the more robust calculation of f^{esc}. Gower et al. (1999) found that the difference between fPAR and $\mathrm{fPAR_{green}}$ diverged between 5% and 35%, though in practice they argued that the difference likely falls on the lower end of this range because leaves tend to preferentially cluster around branches, as opposed to being randomly distributed throughout the canopy (see also, Dufrêne and Bréda, 1995). Such reasoning has empirical support as well. Both Kucharik et al. (1998) and Ryu et al. (2012) found that woody elements of the canopy were largely masked by vegetation, resulting in only small differences between plant area index and leaf area index. While accurately calculating fPAR complicates the global application of Eq. 12, the approach should be more than suitable for *in situ* studies where SIF, $\mathrm{NIR_V}$, and fPAR can be more robustly determined through careful site-level instrumentation. If combined with *in situ* measurements of photosynthesis, these data might help in further elucidating the nature of SIF-$\mathrm{NIR_V}$-photosynthesis relationship.

Alternatively, it should still be possible to use Eq. 12 even without knowing fPAR to normalize SIF to a constant viewing geometry. Cross-sensor combinations of SIF and reflectance data should be possible so long as SIF and optical measurements are made in close succession, such that the fPAR across the two satellite measurements can be assumed constant. While such an approach would enable the normalization of SIF and allow for comparisons of SIF measure-

ments across space, it would not allow the precise calculation of SIF_{Total} due to uncertainty in the true value of fPAR. In this mode, MODIS BRF products might be used to calculate NIR_V and combined with off-nadir SIF and NIR_V observations from TROPOMI or OCO-2 to generate a nadir-normalized SIF dataset. Even more promising is the newly launched EPIC sensor, a high-resolution spectral camera capable of capturing sub-hourly, full-disc images of the Earth at roughly 10 km^2 (Marshak and Knyazikhin, 2017). EPIC is situated such that it stares directly into the hot-spot, which offers two unique advantages. First, constant view geometry and high temporal resolution would allow normalization using near simultaneous observations to the EPIC view, which would eliminate seasonal changes in solar elevation that still complicate nadir-adjusted imagery. Second, looking into the hot-spot means that EPIC mostly sees only fully-illuminated leaves. Sun-lit leaves, in turn, contribute the lion-share of total emitted fluorescence, meaning hot-spot observations of NIR_V may be expected to provide directional-corrected measurements of SIF that strongly correlate with total emitted SIF and in turn provide a strong basis for estimating APAR and GPP globally.

6 Conclusion

The escape ratio between directional SIF and total emitted SIF can influence the SIF-GPP relationship and is determined by the sun-canopy-sensor geometry, canopy structure parameters and leaf/soil optical properties. The widely used radiative transfer forward models require knowledge of canopy structure parameters and leaf/soil optical properties, while the relatively easier BRF_T approach can only be used over dense canopies or against dark soil backgrounds. We developed a simple but accurate approach to estimate the escape ratio, $\frac{NIR_V}{fPAR}$, which effectively removes the influence of soil reflectance and can be easily applied using existing *in situ* or remotely sensed NIR_V and fPAR datasets. The proposed escape ratio formula was evaluated for different canopy structure, soil brightness, and view geometry cases by SCOPE simulations, and achieved higher accuracy than the BRF_T approach.

Acknowledgements

We thank Kaiyu Guan, Ari Kornfeld, Guofang Miao, and Xi Yang for their helpful discussions. Y.Z. was in part supported by the National Key Research and Development Program (No. 2018YFA0605503) and the National Natural Science Foundation of China (No. 41701401) at the beginning of the research. Christian Frankenberg and Philipp Köhler helped in our interpretation of the TROPOMI results and provided the TROPOMI data, which was funded by the EARTH SCIENCE U.S. PARTICIPATING INVESTIGATOR (Grant Number: NNX15AH95G). G.B. was supported by a NASA Earth and Space Science fellowship. B.D. and Y.R. were supported by the National Research Foundation of Korea (NRF-2016M1A3A3A02018195). While writing this paper, Y.R. was supported by the Carnegie Institution for Science during a sabbatical leave. M.C. was supported by a Laboratory Directed Research and Development project sponsored by the Pacific Northwest National Laboratory of the U.S. Department of Energy.

Appendix

Canopy Spectral Invariants Primer

This Appendix provides additional background on canopy spectral invariant theory and how spectral invariant properties (SIP) relate to BRF and f^{esc}. For a complete introduction, see Knyazikhin et al. (2013) and Stenberg et al. (2016). For our purposes, we are more interested in the practical application of SIP to better understand f^{esc}. The three SIP parameters used in our derivation relating $\mathrm{NIR_V}$ and fPAR to f^{esc} are:

1. **Escape probability ($\boldsymbol{\rho_n(\Omega)}$)**: the probability that a solar photon, on its n-th interaction with a vegetated element of the canopy, escapes the canopy in the direction Ω.

2. **Recollision probability ($\boldsymbol{p_n}$)**: the probability that a solar photon, on its n-th interaction with a vegetated element of the canopy, recollides with the canopy an n-th plus one time.

3. **Canopy interceptance ($\boldsymbol{i_0}$)**: the probability that an incoming solar photon interacts with a vegetated element of the canopy.

Importantly, SIP hold for all wavelengths of incoming light. In this sense, SIP allows for canopy radiative transfer to be treated in the abstract, as opposed to requiring detailed knowledge of canopy geometry.

Spectral Invariants and $\boldsymbol{f^{esc}}$

SIP are relevant to the manuscript at hand, as f^{esc} can be described purely in terms of ρ_n, p_n, and the near-infrared (NIR) leaf albedo, ω_N, which although not an invariant property, is relatively invariant across time and space (Asner, 1998; Gates et al., 1965). Using these terms, f^{esc} can be described as:

$$\begin{aligned} f^{esc}_{BS}(\lambda_f, \Omega) = \rho_1(\Omega) \\ &+ p_1 \cdot \omega(\lambda_f) \cdot \rho_2(\Omega) \\ &+ p_1 \cdot \omega(\lambda_f) \cdot p_2 \cdot \omega(\lambda_f) \cdot \rho_3(\Omega) \\ &+ \dots . \end{aligned} \tag{A1}$$

Note that for purposes of this Text, we present all results in terms of the "black soil" condition, which we denote with the subscript "BS." All Equations can be expanded to account for the multiple scattering of a reflective soil background, but are excluded here both for brevity and because $\mathrm{NIR_V}$ closely approximates the BS condition. Furthermore, for Eq. A1, the SIF re-excited by multiple scattered SIF photons are regarded as negligible (<0.1%) (Zhao et al., 2016).

The geometric series in Eq. A1 can be more succinctly written as:

$$f_{BS}^{esc}(\lambda_f, \Omega) = \frac{\rho(\Omega)}{1 - p\omega(\lambda_f)}, \tag{A2}$$

which more directly illustrates the relationship of ρ and p to f^{esc}. As was the case in the Main Text, Eq. A2 can again be simplified if ω_N is assumed to equal 1. Of course, precise knowledge of ω_N would improve estimates of f^{esc}. Furthermore, the linearity of $\mathrm{NIR_V}$ and f^{esc} by Eq. 12 from the Main Text underscores our claim that $\mathrm{NIR_V}$ represents a new tool for exploring SIP at large scales.

The Directional Area Scattering Factor

SIP also allow use to describe the relationship between SIF, f^{esc}, and $\mathrm{NIR_V}$ in slightly more comprehensive terms. The following Equations were helpful in our own exploration of the $\mathrm{NIR_V}$-f^{esc} relationship and, for this reason, we present them here.

The three SIP outlined above combine together to form a parameter known as the directional area scattering factor (DASF):

$$DASF = \frac{\rho(\Omega) i_0}{1 - p}, \tag{A3}$$

which fully describes the canopy radiative transfer environment. Below, we use DASF as a bridging term between f^{esc}, directional SIF, and $\mathrm{NIR_V}$. We do this by describing each of these variables in terms of DASF.

We start by relating f^{esc} to DASF, which requires only a slight modification of Eq. A2. By slightly rearranging how we reduce the Neumann series presented in Eq. A1 and simultaneously multiplying and dividing by i_0, we get:

$$
\begin{aligned}
f_{BS}^{esc}(\lambda_f, \Omega) &= \frac{\rho(\Omega)}{1 - p\omega(\lambda_f)} \\
&= \frac{\rho(\Omega) i_0}{1-p} \cdot \frac{1-p}{1 - p\omega(\lambda_f)} \cdot \frac{1}{i_0} \\
&\approx DASF \cdot \frac{1}{i_0}.
\end{aligned} \tag{A4}
$$

Next, we can describe directional SIF as a function of total emitted SIF and the escape ratio. The total emitted SIF by all leaves within the canopy can be written as:

$$
SIF_{Total}(\lambda_f) = i_0 \int_{400}^{750} Q_{dir}(\lambda_e) \cdot M(\lambda_e, \lambda_f) \cdot \Phi'_F d\lambda_e \tag{A5}
$$

where $\mathrm{Q_{dir}}(\lambda_e)$ is incoming photon flux density at wavelength λ_e (we ignore diffuse radiation for now), $M(\lambda_e, \lambda_f)$ is the leaf fluorescence excitation-emission matrix where rows represent the excitation wavelength λ_e from 400 to 750 nm, and columns represent the emission wavelength λ_f from 640 to 850 nm (van der Tol et al., 2009). $M(\lambda_e, \lambda_f)$ is linearly scaled with the amplification factor Φ'_F which is PAR-dependent and can vary throughout the canopy. $\mathrm{SIF_{Total}}$ becomes directional SIF ($\mathrm{SIF}(\Omega)$) by accounting for f^{esc}:

$$
SIF(\lambda_f, \Omega) = SIF_{Total}(\lambda_f) \cdot f_{BS}^{esc}(\lambda_f, \Omega), \tag{A6}
$$

which can be fully expanded to:

$$
\begin{aligned}
SIF(\lambda_f, \Omega) &= \frac{\rho(\Omega) i_0}{1-p} \cdot \left[\frac{1-p}{1 - p\omega(\lambda_f)} \int_{400}^{750} Q_{dir}(\lambda_e) \cdot M(\lambda_e, \lambda_f) \cdot \Phi'_F d\lambda_e \right] \\
&= DASF \cdot CES.
\end{aligned} \tag{A7}
$$

Eq. A7 neatly partitions SIF into two components: the purely structural/radiative transform component represented by DASF and what we call the canopy emission-scattering (CES) coefficient, which relates to leaf biochemical properties by $M(\lambda_e, \lambda_f)$, incident radiation $Q_{\mathrm{dir}}(\lambda_e)$, and electron transport via Φ'_F.

The final step in relating $\mathrm{NIR_V}$ to f^{esc} via DASF is describing $\mathrm{BRF_V}$ in terms of DASF. This step has previously been described by Knyazikhin et al. (2013) in the same paper in which DASF

was first introduced:

$$
\begin{aligned}
BRF_V(\lambda_f, \Omega) &= \frac{\rho(\Omega) i_0}{1-p} \cdot \left[\frac{1-p}{1-p\omega(\lambda_f)} \omega(\lambda_f) \right] \\
&= DASF \cdot CSC.
\end{aligned}
\tag{A8}
$$

As was the case in Eq. A7, this rearrangement separates structural concerns (encapsulated by DASF) and the canopy scattering coefficient (CSC), which relates to leaf albedo (see also, Köhler et al., 2018).

With this, all the pieces are in place for relating $\mathrm{NIR_V}$, SIF, and f^{esc} to each other via DASF. To fully complete the circle, from Eqs. A4, A8 and 10 from the Main Text, we can write:

$$
\begin{aligned}
DASF &= \frac{NIR_{\mathrm{V}}}{CSC} \\
&\approx \frac{NIR_{\mathrm{V}}}{\omega_N}.
\end{aligned}
\tag{A9}
$$

References

Asner, G. P. (1998). "Biophysical and biochemical sources of variability in canopy reflectance". *Remote Sensing of Environment* 64.3, pp. 234–253.

Atherton, J., B. Olascoaga, L. Alonso, and A. Porcar-Castell (2017). "Spatial variation of leaf optical properties in a boreal forest is influenced by species and light environment". *Frontiers in Plant Science* 8, p. 309.

Badgley, G., C. B. Field, and J. A. Berry (2017). "Canopy near-infrared reflectance and terrestrial photosynthesis". *Science Advances* 3.3, e1602244.

Baret, F., V. C. Vanderbilt, M. D. Steven, and S. Jacquemoud (1994). "Use of spectral analogy to evaluate canopy reflectance sensitivity to leaf optical properties". *Remote Sensing of Environment* 48.2, pp. 253–260.

Chen, J. M. (1996). "Optically-based methods for measuring seasonal variation of leaf area index in boreal conifer stands". *Agricultural and Forest Meteorology* 80.2-4, pp. 135–163.

Drusch, M., J. Moreno, U. Del Bello, R. Franco, Y. Goulas, A. Huth, S. Kraft, E. M. Middleton, F. Miglietta, G. Mohammed, et al. (2017). "The FLuorescence EXplorer Mission Concept—ESA's Earth Explorer 8". *IEEE Transactions on Geoscience and Remote Sensing* 55.3, pp. 1273–1284.

Du, S., L. Liu, X. Liu, and J. Hu (2017). "Response of canopy solar-induced chlorophyll fluorescence to the absorbed photosynthetically active radiation absorbed by chlorophyll". *Remote Sensing* 9.9, p. 911.

Dufrêne, E. and N. Bréda (1995). "Estimation of deciduous forest leaf area index using direct and indirect methods". *Oecologia* 104.2, pp. 156–162.

Fournier, A., F. Daumard, S. Champagne, A. Ounis, Y. Goulas, and I. Moya (2012). "Effect of canopy structure on sun-induced chlorophyll fluorescence". *ISPRS Journal of Photogrammetry and Remote Sensing* 68, pp. 112–120.

Frankenberg, C., A. Butz, and G. Toon (2011a). "Disentangling chlorophyll fluorescence from atmospheric scattering effects in O2 A-band spectra of reflected sun-light". *Geophysical Research Letters* 38.3.

Frankenberg, C., J. B. Fisher, J. Worden, G. Badgley, S. S. Saatchi, J.-E. Lee, G. C. Toon, A. Butz, M. Jung, A. Kuze, et al. (2011b). "New global observations of the terrestrial carbon cy-

cle from GOSAT: Patterns of plant fluorescence with gross primary productivity". *Geophysical Research Letters* 38.17.

Gastellu-Etchegorry, J.-P., N. Lauret, T. Yin, L. Landier, A. Kallel, Z. Malenovsk, A. Al Bitar, J. Aval, S. Benhmida, J. Qi, et al. (2017). "DART: Recent advances in remote sensing data modeling with atmosphere, polarization, and chlorophyll fluorescence". *IEEE Journal of Selected Topics in Applied Earth Observations and Remote Sensing* 10.6, pp. 2640–2649.

Gastellu-Etchegorry, J., E. Martin, and F. Gascon (2004). "DART: a 3D model for simulating satellite images and studying surface radiation budget". *International journal of remote sensing* 25.1, pp. 73–96.

Gates, D. M., H. J. Keegan, J. C. Schleter, and V. R. Weidner (1965). "Spectral properties of plants". *Applied Optics* 4.1, pp. 11–20.

Gitelson, A. A., C. Buschmann, and H. K. Lichtenthaler (1998). "Leaf chlorophyll fluorescence corrected for re-absorption by means of absorption and reflectance measurements". *Journal of Plant Physiology* 152.2-3, pp. 283–296.

Gobron, N. (2010). "Ocean and Land Colour Instrument (OLCI) FAPAR and Rectified Channels over Terrestrial Surfaces Algorithm Theoretical Basis Document. EUR Report No. xxxxx EN". *European Commission Joint Research Centre (JRC) Scientific and Technical Reports*.

Gower, S. T., C. J. Kucharik, and J. M. Norman (1999). "Direct and indirect estimation of leaf area index, fAPAR, and net primary production of terrestrial ecosystems". *Remote sensing of environment* 70.1, pp. 29–51.

Guanter, L., C. Frankenberg, A. Dudhia, P. E. Lewis, J. Gómez-Dans, A. Kuze, H. Suto, and R. G. Grainger (2012). "Retrieval and global assessment of terrestrial chlorophyll fluorescence from GOSAT space measurements". *Remote Sensing of Environment* 121, pp. 236–251.

Guanter, L., Y. Zhang, M. Jung, J. Joiner, M. Voigt, J. A. Berry, C. Frankenberg, A. R. Huete, P. Zarco-Tejada, J.-E. Lee, et al. (2014). "Global and time-resolved monitoring of crop photosynthesis with chlorophyll fluorescence". *Proceedings of the National Academy of Sciences*, p. 201320008.

He, L., J. M. Chen, J. Liu, G. Mo, and J. Joiner (2017). "Angular normalization of GOME-2 Sun-induced chlorophyll fluorescence observation as a better proxy of vegetation productivity". *Geophysical Research Letters* 44.11, pp. 5691–5699.

Hernández-Clemente, R., P. R. North, A. Hornero, and P. J. Zarco-Tejada (2017). "Assessing the effects of forest health on sun-induced chlorophyll fluorescence using the FluorFLIGHT 3-D radiative transfer model to account for forest structure". *Remote Sensing of Environment* 193, pp. 165–179.

Huang, D., Y. Knyazikhin, R. E. Dickinson, M. Rautiainen, P. Stenberg, M. Disney, P. Lewis, A. Cescatti, Y. Tian, W. Verhoef, et al. (2007). "Canopy spectral invariants for remote sensing and model applications". *Remote Sensing of Environment* 106.1, pp. 106–122.

Jacquemoud, S. and F. Baret (1990). "PROSPECT: A model of leaf optical properties spectra". *Remote sensing of environment* 34.2, pp. 75–91.

Knyazikhin, Y., J. Martonchik, R. B. Myneni, D. Diner, and S. W. Running (1998). "Synergistic algorithm for estimating vegetation canopy leaf area index and fraction of absorbed photosynthetically active radiation from MODIS and MISR data". *Journal of Geophysical Research: Atmospheres* 103.D24, pp. 32257–32275.

Knyazikhin, Y., M. A. Schull, P. Stenberg, M. Mõttus, M. Rautiainen, Y. Yang, A. Marshak, P. L. Carmona, R. K. Kaufmann, P. Lewis, et al. (2013). "Hyperspectral remote sensing of foliar nitrogen content". *Proceedings of the National Academy of Sciences* 110.3, E185–E192.

Köhler, P., C. Frankenberg, T. S. Magney, L. Guanter, J. Joiner, and J. Landgraf (2018). "Global Retrievals of Solar-Induced Chlorophyll Fluorescence With TROPOMI: First Results and Intersensor Comparison to OCO-2". *Geophysical Research Letters* 45.19, pp. 10–456.

Krause, G. and E. Weis (1991). "Chlorophyll fluorescence and photosynthesis: the basics". *Annual Review of Plant Biology* 42.1, pp. 313–349.

Kucharik, C. J., J. M. Norman, and S. T. Gower (1998). "Measurements of branch area and adjusting leaf area index indirect measurements". *Agricultural and Forest Meteorology* 91.1-2, pp. 69–88.

Liu, L., X. Liu, Z. Wang, and B. Zhang (2016). "Measurement and analysis of bidirectional SIF emissions in wheat canopies". *IEEE Transactions on Geoscience and Remote Sensing* 54.5, pp. 2640–2651.

Liu, X., L. Guanter, L. Liu, A. Damm, Z. Malenovský, U. Rascher, D. Peng, S. Du, and J.-P. Gastellu-Etchegorry (2018). "Downscaling of solar-induced chlorophyll fluorescence from canopy level to photosystem level using a random forest model". *Remote Sensing of Environment*.

Malenovský, Z., K. B. Mishra, F. Zemek, U. Rascher, and L. Nedbal (2009). "Scientific and technical challenges in remote sensing of plant canopy reflectance and fluorescence". *Journal of Experimental Botany* 60.11, pp. 2987–3004.

Marshak, A. and Y. Knyazikhin (2017). "The spectral invariant approximation within canopy radiative transfer to support the use of the EPIC/DSCOVR oxygen B-band for monitoring vegetation". *Journal of Quantitative Spectroscopy and Radiative Transfer* 191, pp. 7–12.

Miao, G., K. Guan, X. Yang, C. J. Bernacchi, J. A. Berry, E. H. DeLucia, J. Wu, C. E. Moore, K. Meacham, Y. Cai, et al. (2018). "Sun-Induced Chlorophyll Fluorescence, Photosynthesis, and Light Use Efficiency of a Soybean Field from Seasonally Continuous Measurements". *Journal of Geophysical Research: Biogeosciences* 123.2, pp. 610–623.

Migliavacca, M., O. Perez-Priego, M. Rossini, T. S. El-Madany, G. Moreno, C. van der Tol, U. Rascher, A. Berninger, V. Bessenbacher, A. Burkart, et al. (2017). "Plant functional traits and canopy structure control the relationship between photosynthetic CO 2 uptake and far-red sun-induced fluorescence in a Mediterranean grassland under different nutrient availability". *New Phytologist* 214.3, pp. 1078–1091.

Mu, X., R. Hu, Y. Zeng, T. R. McVicar, H. Ren, W. Song, Y. Wang, R. Casa, J. Qi, D. Xie, et al. (2017). "Estimating structural parameters of agricultural crops from ground-based multi-angular digital images with a fractional model of sun and shade components". *Agricultural and Forest Meteorology* 246, pp. 162–177.

Porcar-Castell, A. (2011). "A high-resolution portrait of the annual dynamics of photochemical and non-photochemical quenching in needles of Pinus sylvestris". *Physiologia Plantarum* 143.2, pp. 139–153.

Porcar-Castell, A., E. Tyystjärvi, J. Atherton, C. van der Tol, J. Flexas, E. E. Pfündel, J. Moreno, C. Frankenberg, and J. A. Berry (2014). "Linking chlorophyll a fluorescence to photosynthesis for remote sensing applications: mechanisms and challenges". *Journal of Experimental Botany* 65.15, pp. 4065–4095.

Qi, J., A. Chehbouni, A. Huete, Y. Kerr, and S. Sorooshian (1994). "A modified soil adjusted vegetation index". *Remote Sensing of Environment* 48.2, pp. 119–126.

Raabe, K., J. Pisek, O. Sonnentag, and K. Annuk (2015). "Variations of leaf inclination angle distribution with height over the growing season and light exposure for eight broadleaf tree species". *Agricultural and Forest Meteorology* 214, pp. 2–11.

Ramos, M. E. and M. G. Lagorio (2006). "A model considering light reabsorption processes to correct in vivo chlorophyll fluorescence spectra in apples". *Photochemical & Photobiological Sciences* 5.5, pp. 508–512.

Romero, J. M., G. B. Cordon, and M. G. Lagorio (2018). "Modeling re-absorption of fluorescence from the leaf to the canopy level". *Remote Sensing of Environment* 204, pp. 138–146.

Ross, J. (1981). *The radiation regime and architecture of plant stands*. Dr W. Junk Publishers.

Ryu, Y., O. Sonnentag, T. Nilson, R. Vargas, H. Kobayashi, R. Wenk, and D. D. Baldocchi (2010). "How to quantify tree leaf area index in an open savanna ecosystem: a multi-instrument and multi-model approach". *Agricultural and Forest Meteorology* 150.1, pp. 63–76.

Ryu, Y., J. Verfaillie, C. Macfarlane, H. Kobayashi, O. Sonnentag, R. Vargas, S. Ma, and D. D. Baldocchi (2012). "Continuous observation of tree leaf area index at ecosystem scale using upward-pointing digital cameras". *Remote Sensing of Environment* 126, pp. 116–125.

Schaaf, C. B., F. Gao, A. H. Strahler, W. Lucht, X. Li, T. Tsang, N. C. Strugnell, X. Zhang, Y. Jin, J.-P. Muller, et al. (2002). "First operational BRDF, albedo nadir reflectance products from MODIS". *Remote sensing of Environment* 83.1-2, pp. 135–148.

Smith, W., J. Biederman, R. Scott, D. Moore, M. He, J. Kimball, D. Yan, A. Hudson, M. Barnes, N. MacBean, et al. (2018). "Chlorophyll fluorescence better captures seasonal and interannual gross primary productivity dynamics across dryland ecosystems of southwestern North America". *Geophysical Research Letters* 45.2, pp. 748–757.

Smolander, S. and P. Stenberg (2005). "Simple parameterizations of the radiation budget of uniform broadleaved and coniferous canopies". *Remote Sensing of Environment* 94.3, pp. 355–363.

Song, W., X. Mu, G. Ruan, Z. Gao, L. Li, and G. Yan (2017). "Estimating fractional vegetation cover and the vegetation index of bare soil and highly dense vegetation with a physically based method". *International Journal of Applied Earth Observation and Geoinformation* 58, pp. 168–176.

Stenberg, P., M. Mõttus, and M. Rautiainen (2016). "Photon recollision probability in modelling the radiation regime of canopies—A review". *Remote Sensing of Environment* 183, pp. 98–108.

Sun, Y., C. Frankenberg, M. Jung, J. Joiner, L. Guanter, P. Köhler, and T. Magney (2018). "Overview of Solar-Induced chlorophyll Fluorescence (SIF) from the Orbiting Carbon Observatory-2: Re-

trieval, cross-mission comparison, and global monitoring for GPP". *Remote Sensing of Environment* 209, pp. 808–823.

Sun, Y., C. Frankenberg, J. D. Wood, D. S. Schimel, M. Jung, L. Guanter, D. Drewry, M. Verma, A. Porcar-Castell, T. J. Griffis, et al. (2017). "OCO-2 advances photosynthesis observation from space via solar-induced chlorophyll fluorescence". *Science* 358.6360, eaam5747.

Tucker, C. J. (1979). "Red and photographic infrared linear combinations for monitoring vegetation". *Remote Sensing of Environment* 8.2, pp. 127–150.

van der Tol, C., J. Berry, P. Campbell, and U. Rascher (2014). "Models of fluorescence and photosynthesis for interpreting measurements of solar-induced chlorophyll fluorescence". *Journal of Geophysical Research: Biogeosciences* 119.12, pp. 2312–2327.

van der Tol, C., W. Verhoef, J. Timmermans, A. Verhoef, and Z. Su (2009). "An integrated model of soil-canopy spectral radiances, photosynthesis, fluorescence, temperature and energy balance". *Biogeosciences* 6.12, pp. 3109–3129.

van der Tol, C., M. Rossini, S. Cogliati, W. Verhoef, R. Colombo, U. Rascher, and G. Mohammed (2016). "A model and measurement comparison of diurnal cycles of sun-induced chlorophyll fluorescence of crops". *Remote sensing of environment* 186, pp. 663–677.

Veefkind, J., I. Aben, K. McMullan, H. Förster, J. De Vries, G. Otter, J. Claas, H. Eskes, J. De Haan, Q. Kleipool, et al. (2012). "TROPOMI on the ESA Sentinel-5 Precursor: A GMES mission for global observations of the atmospheric composition for climate, air quality and ozone layer applications". *Remote Sensing of Environment* 120, pp. 70–83.

Verhoef, W. (1984). "Light scattering by leaf layers with application to canopy reflectance modeling: the SAIL model". *Remote sensing of environment* 16.2, pp. 125–141.

Vilfan, N., C. van der Tol, O. Muller, U. Rascher, and W. Verhoef (2016). "Fluspect-B: A model for leaf fluorescence, reflectance and transmittance spectra". *Remote Sensing of Environment* 186, pp. 596–615.

Yang, K., Y. Ryu, B. Dechant, J. A. Berry, Y. Hwang, C. Jiang, M. Kang, J. Kim, H. Kim, A. Kornfeld, and X. Yang (2018). "Sun-induced chlorophyll fluorescence is more strongly related to absorbed light than to photosynthesis at half-hourly resolution in a rice paddy". *Remote Sensing of Environment* 216, pp. 658–673.

Yang, P. and C. van der Tol (2018). "Linking canopy scattering of far-red sun-induced chlorophyll fluorescence with reflectance". *Remote Sensing of Environment* 209, pp. 456–467.

Yang, X., J. Tang, J. F. Mustard, J.-E. Lee, M. Rossini, J. Joiner, J. W. Munger, A. Kornfeld, and A. D. Richardson (2015). "Solar-induced chlorophyll fluorescence that correlates with canopy photosynthesis on diurnal and seasonal scales in a temperate deciduous forest". *Geophysical Research Letters* 42.8, pp. 2977–2987.

Zhang, Q., X. Xiao, B. Braswell, E. Linder, F. Baret, and B. Moore III (2005). "Estimating light absorption by chlorophyll, leaf and canopy in a deciduous broadleaf forest using MODIS data and a radiative transfer model". *Remote Sensing of Environment* 99.3, pp. 357–371.

Zhang, Y., L. Guanter, J. A. Berry, C. van der Tol, X. Yang, J. Tang, and F. Zhang (2016). "Model-based analysis of the relationship between sun-induced chlorophyll fluorescence and gross primary production for remote sensing applications". *Remote sensing of environment* 187, pp. 145–155.

Zhao, F., X. Dai, W. Verhoef, Y. Guo, C. van der Tol, Y. Li, and Y. Huang (2016). "FluorWPS: a Monte Carlo ray-tracing model to compute sun-induced chlorophyll fluorescence of three-dimensional canopy". *Remote Sensing of Environment* 187, pp. 385–399.

Glossary

ABS_V: canopy absorbance of visible light

BRF: bidirectional reflectance factor

BRF_T: the total scene bidirectional reflectance factor

BRF_V: contribution to BRF_T of photons reflected off only the scene's vegetative component

BRF_S: contribution to BRF_T of photons reflected off soil alone

BRF_M: contribution to BRF_T of photons from multiple scattering between the vegetation and soil

BS: black soil problem

CES: Canopy Emission/Scattering coefficient

CSC: Canopy Scattering Coefficient

DASF: Directional Area Scattering Factor

FVC: fractional vegetation cover

F_V: the fraction of $\mathrm{NIR_T}$ that originates from interactions with vegetation alone

F_S: the fraction of $\mathrm{NIR_T}$ that originates from interactions with soil alone

F_M: the fraction of $\mathrm{NIR_T}$ that originates from the multiple scattering between the vegetation and soil

$fPAR$: the fraction of absorbed photosynthetically active radiation

$f\mathrm{PAR_{chl}}$: the fraction of PAR absorbed by chlorophyll

$f^{\mathrm{esc}}(\lambda_f, \Omega)$: escape ratio, which is the fraction of SIF photons at a given wavelength (λ_f) that ultimately escape the canopy and are observed at the view angle of Ω

Φ_F: the quantum yield of fluorescence

Φ'_F: the amplification factor of the quantum yield of fluorescence

i_0: canopy interceptance, which is the probability that an incoming solar photon interacts with a vegetated element of the canopy

LAI: leaf area index

$M\left(\lambda_e, \lambda_f\right)$: he leaf fluorescence excitation-emission matrix where rows represent the excitation wavelength λ_e from 400 to 750 nm, and columns represent the emission wavelength λ_f from 640 to 850nm

NDVI: the normalized difference vegetation index

NIR_T: shorthand for $\mathrm{BRF}_T(NIR)$

$\mathrm{NIR}_T^{'}$: the total NIR radiance reflected by the land surface

NIR_V: the NIR reflectance of vegetation, which can be calculated by $NDVI \bullet \mathrm{NIR}_T$ and is an approximation of $\mathrm{BRF}_V(NIR)$

$\mathrm{NIR}_V^{'}$: the total NIR radiance reflected by the vegetated component of the land surface

NIR_S: contribution to NIR_T of photons reflected off soil alone

NIR_M: contribution to NIR_T of photons from multiple scattering between the vegetation and soil

PAR: absorbed photosynthetically active radiation

$\rho_n(\Omega)$: Escape probability, which is the probability that a solar photon, on its n-th interaction with a vegetated element of the canopy, escapes the canopy in the direction Ω

p_n: Recollision probability, which is the probability that a solar photon, on its n-th interaction with a vegetated element of the canopy, recollides with the canopy an n-th plus one time.

$Q_{\mathrm{dir}}(\lambda_e)$: the direct incoming photon flux density at wavelength λ_e

S_λ: the flux of incoming solar radiation at wavelength λ

SIF: solar-induced chlorophyll fluorescence

$\mathrm{SIF}_{\mathrm{Total}}(\lambda_f)$: the sum of all SIF photons at a given wavelength (λ_f) emitted by all leaves within the canopy in all directions

$\mathrm{SIF}_{\mathrm{Obs}}(\lambda_f, \Omega)$: SIF radiance observed at the top of canopy at a given wavelength (λ_f) and at the view angle of Ω

SIP: spectral invariant properties

ω_{λ_f}: leaf single scattering albedo at wavelength λ_f

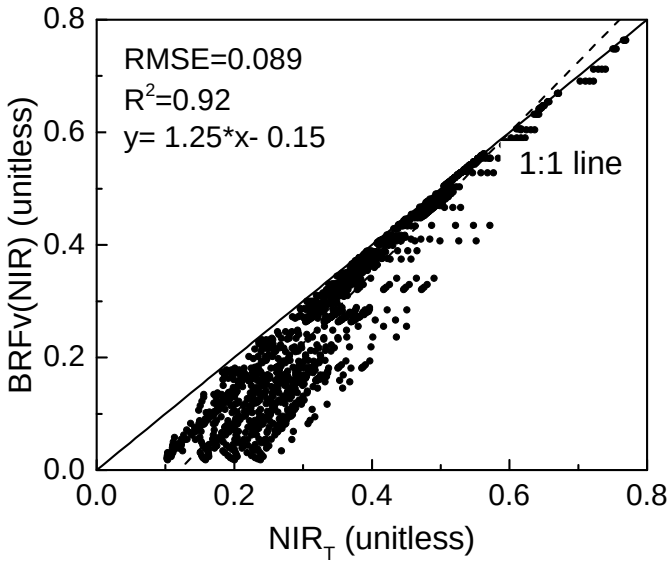

Figure S1: The relationship between whole-scene NIR reflectance, NIR_T, and BRF_V in the near-infrared. NIR_T is mostly linear with BRF_V, except for when FVC is low.

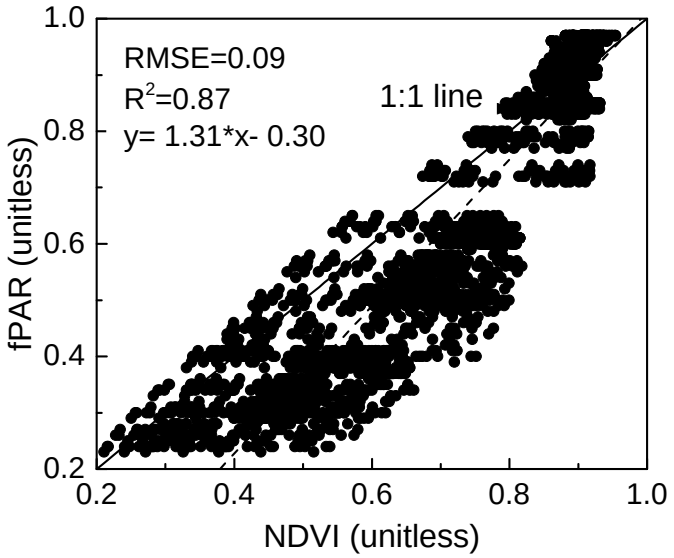

Figure S2: The relationship between NDVI and fPAR. While mostly linear, NDVI and fPAR have different responses to changes in canopy structural parameters. All data generated using the SCOPE simulations outlined in Table 1.

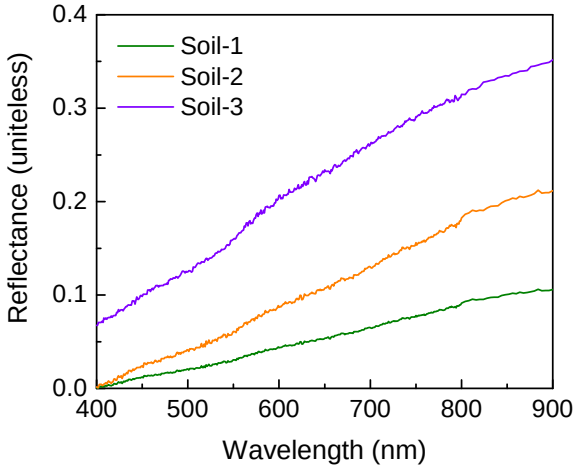

Figure S3: The three soil spectra used examined in the DART simulations. Note the difference in NDVI of the three soil spectra.

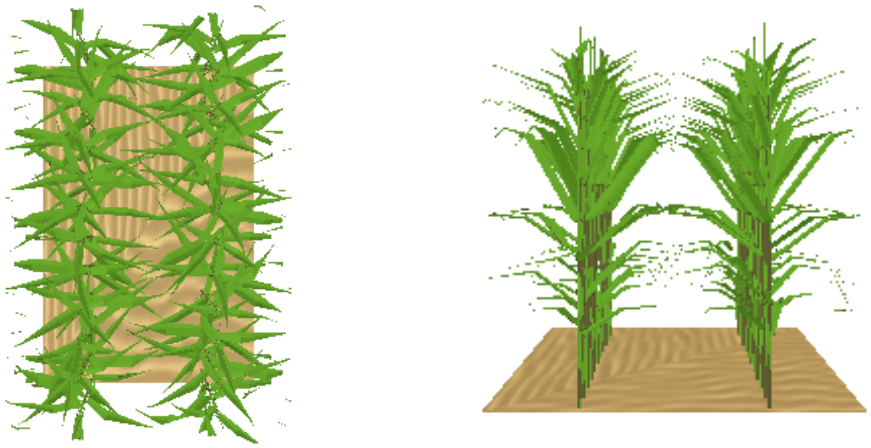

(a) (b)

Figure S4: A) Nadir and B) side views of the three-dimensional canopy used to generate Figs. 5 and 6.

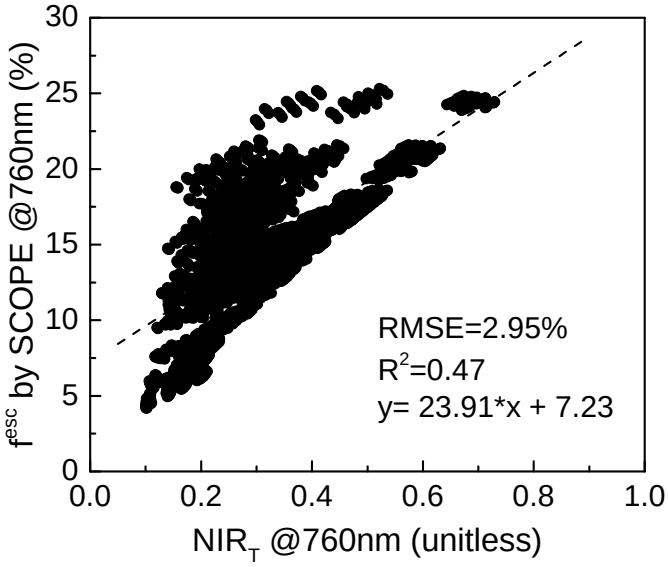

Figure S5: The relationship of $\mathbf{NIR_T}$ and f^{esc} of SIF. $\mathrm{NIR_T}$ alone is a poor predictor of f^{esc} due to the effects of soil contamination.

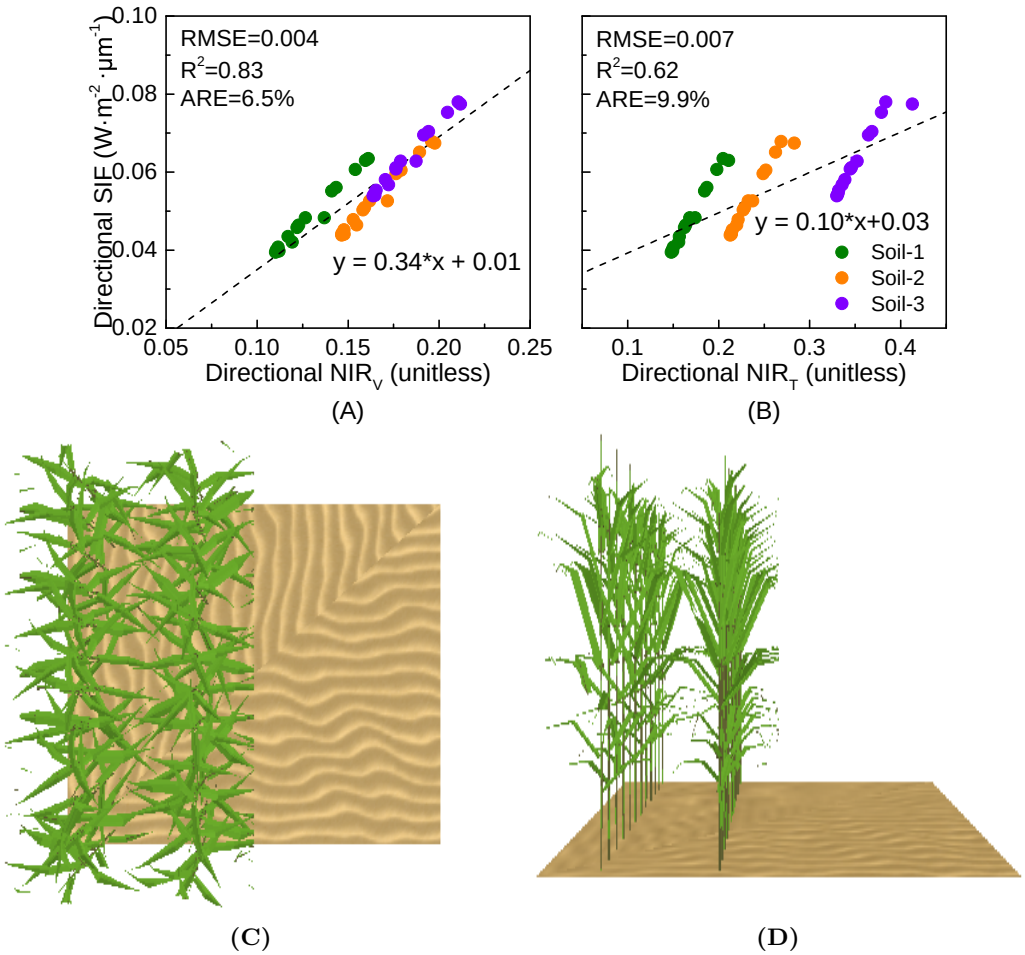

Figure S6: The relationship between directional observations of A) NIR_V and B) NIR_T for a non-uniform (top-view, C & side-view, D), 3-D canopy simulated by DART. When soil constitutes a large fraction of the scene, the influence of BRF_S over NIR_T results in a large reduction in the linearity of the SIF-NIR_T relationship.

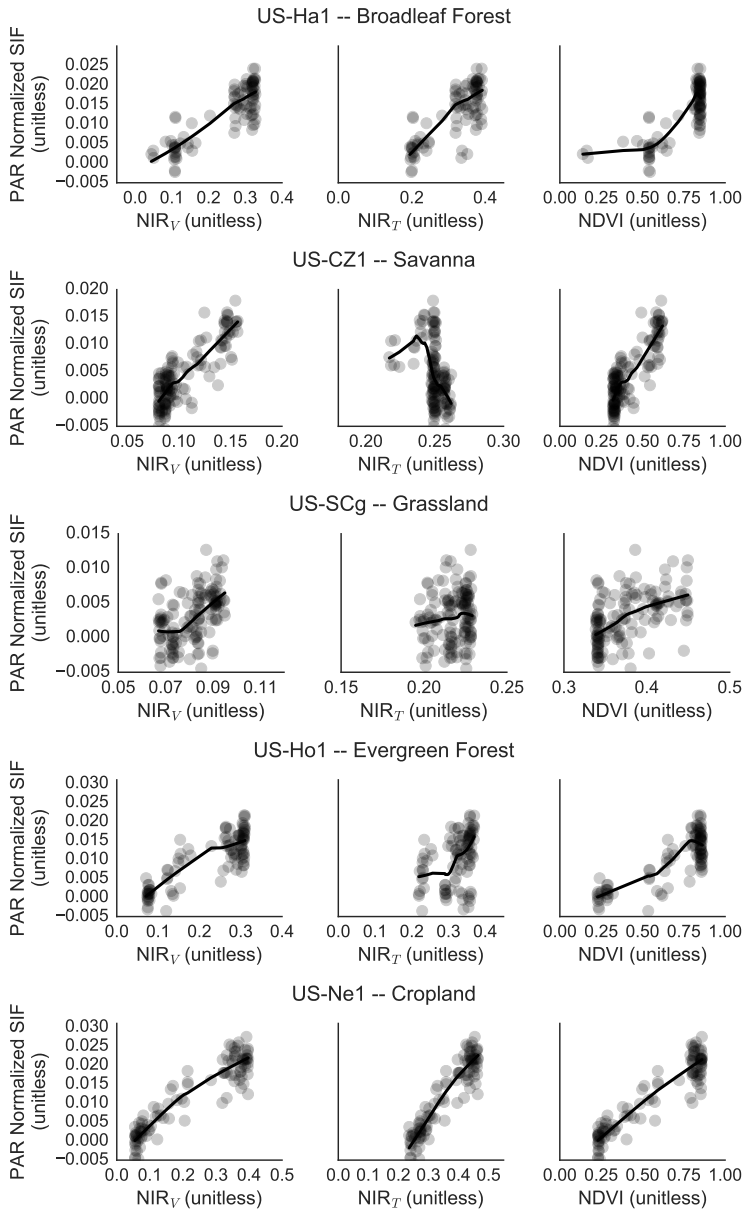

Figure S7: Comparison of NIR$_V$, NIR$_T$, and NDVI against radiation-normalized SIF at five sites across North America. Reflectance data from MODIS MCD43A4. SIF data from TROPOMI.

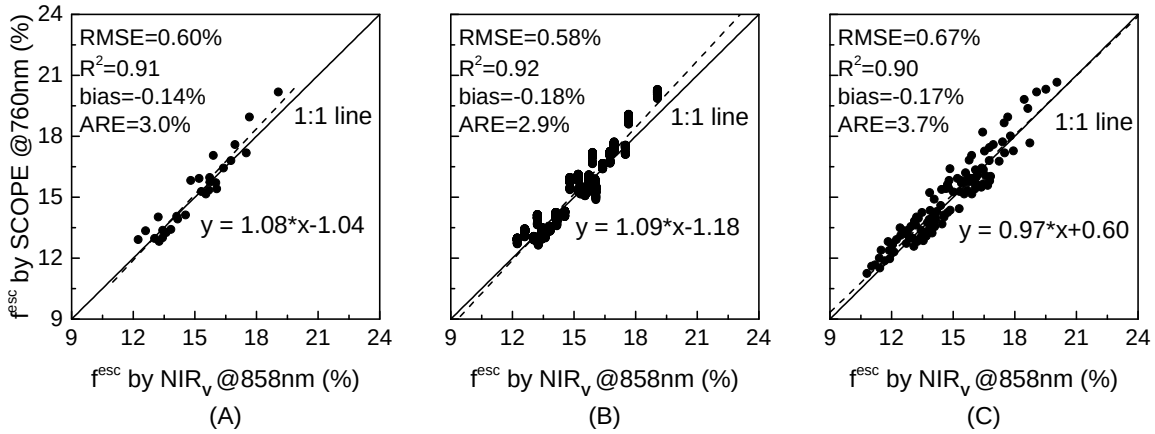

Figure S8: SCOPE simulations comparing a A) baseline scenario with B) simulations designed to only vary Φ_F and C) simulations that vary ω_N. Differences in Φ_F and ω_N cause only slight decoupling of the f^{esc} of SIF relative to the f^{esc} of $\mathrm{NIR_V}$. All data generated using SCOPE, with parameter ranges described in Table S1

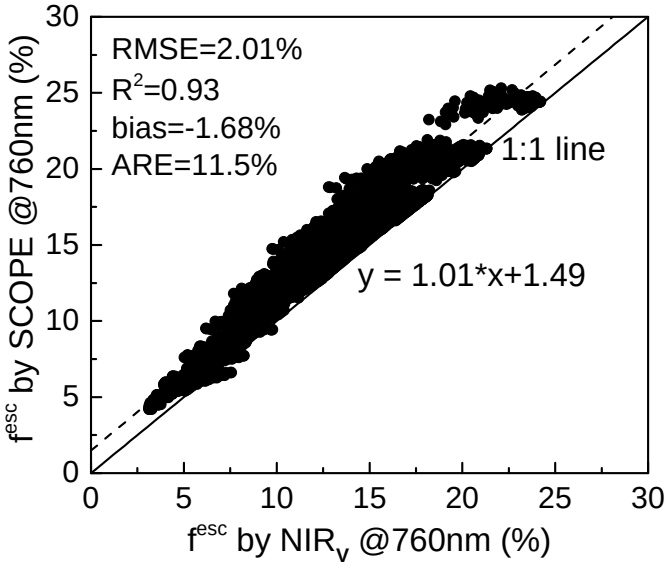

Figure S9: f^{esc} from $\mathbf{NIR_V}$ is more linear with f^{esc} of SIF when both are measured at the same wavelength. For purposes of atmospheric correction, however, NIR reflectance is often measured at longer wavelengths (greater than 800 nm).

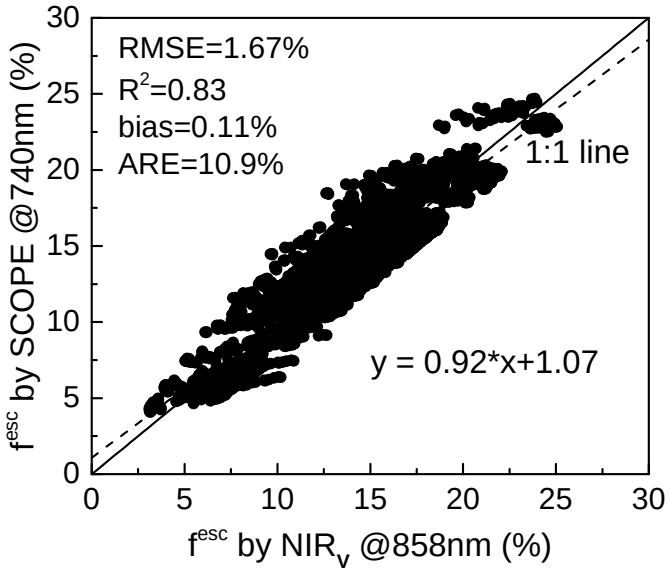

Figure S10: f^{esc} of SIF at 740 nm is more affected by within-canopy reabsorption of SIF photons by chlorophyll than SIF photons emitted at 760 nm, weakening the predictive power of f^{esc} by $\mathrm{NIR_V}$. Correcting such effects requires incorporating information about canopy chlorophyll content into SIF retrievals.

	Variables	Values
Baseline (Figure S8A)	Leaf area index (LAI)	0.5, 1, 3, 5
	View zenith angle	0°, 10°, 20°, 30°, 40°, 50°, 60°
Meteorology & Biochemistry (Φ_F Experiment; Figure S8B)	V_{Cmax}	60, 120
	Vertical V_{Cmax} extinction (kV)	0.6396, 0.85
	Shortwave radiation (Rin)	600, 1200
	Air temperature (Ta)	20, 40
	Air pressure (p)	970, 1090
Leaf Scattering (ω_N Experiment; Figure S8C)	Dry matter content (Cdm)	0.012, 0.024
	Leaf thickness (N)	1.4, 1.8

Table S1: SCOPE parameters and their ranges that were varied for the experiment to study differences in f^{esc} caused by Φ_F and ω_N. Overall, the effects are quite small. All unlisted parameters were kept at their default value in SCOPE v1.70.